



**NTNU – Trondheim**  
Norwegian University of  
Science and Technology

# Exploration of Micro-Doppler Signatures Associated with Humans and Dogs using UWB Radar

**Thor Øyvind Fossum**

Master of Science in Electronics

Submission date: July 2015

Supervisor: Lars Magne Lundheim, IET

Co-supervisor: Jan Roar Pleym, Novelda AS

Norwegian University of Science and Technology  
Department of Electronics and Telecommunications



# Abstract

The work in this thesis has been a part of the task of using a radar to separate between humans and animals in a alarm and surveillance context. For the radar to be able to separate between humans and animals it would use a classifier that rely on features extracted from the radar data. The thesis considers two types of targets; either a human or a dog, and by using micro-Doppler signature, determines some fundamental features which can be the used to classify them. The micro-Doppler signature is the superposition of frequency modulations represented in the joint time and Doppler frequency domain, where the modulations are caused by different moving components associated with the desired target. The micro-Doppler signature has been widely used for radar classification.

The thesis has succeeded in developing algorithms and a system to extract micro-Doppler signatures from targets. Signatures from both humans and dogs has been produced and some simple features extracted from them. The major problem with the signatures created is that the radars pulse repetition frequency is a limiting factor and causes aliasing in the Doppler spectrum that corrupts the signatures. This has limited the study of targets to slow moving humans and dogs.

Three important features for classification was extracted from the micro-Doppler signature by calculating the gait-Doppler map. They are, i) the average Doppler frequency  $f_{av}$ (or average radial velocity  $v_{av}$ ), ii) fundamental gait frequency  $f_g$  and iii) the stride length  $L_s$  which is derived from the two former features.

The result points towards the possibility to separate humans and dogs using these parameters. The reason is that since the dogs limbs are shorter than a human it also has shorter stride length at a specific speed. However, this may not be sufficient for decisions to be made in a robust alarm system, since it can be fooled by a smart intruder that could for example take unnatural short steps and simulate a dogs combination of the aforementioned features.

In addition the determination of features are sensitive to large changes in radial speed. This can be mitigated by preprocessing before the calculation of the features.

The conclusion is, that based on substantial measurements of signatures ( approx. 50 series) and calculations of the three features one has arrived at a fairly robust method to distinguish between the two type of target in this thesis.

# Sammendrag

Denne masteroppgaven fokuserer på en del av det større problemet med å benytte radar til å idenifisere og skille mellom ulike observerte mål i forbindelse med alarm og overvåkingssystemer. Oppgaven fokuserer da på to typisk mål som er relevant ifm hus alarm/overvåkingssystemer; menneske og hund. For å kunne separere mellom mennesker og dyr så må man basere seg på spesifikke egenskaper som identifiserer målet. Ved å benytte mikro-Doppler effekten kan dette oppnås. Mikro-Doppler signatur fremkommer ved en superposisjon av ulike frekvensmodulasjoner både i tid og frekvens, hvor modulasjonene er et resultat av forskjellige bevegelses komponenter generert av målet. Teknikk er kjent i utgangspunktet og benyttet i en rekke anvendelser.

I denne masteroppgaven er det utviklet algoritmer satt i et system for å ekstrahere mikro-Doppler signaturer fra mål. Man har gjennomført en rekke målinger som gir grunnlag for beregne spesifikke egenskaper. Hovedproblemet med å beregne signaturer er radarens puls repetisjonsfrekvens er begrenset og vil for hurtige bevegelser gi opphav til aliasing. Dermed er analysen begrenset til sakt bevegelig mål.

Tre sentrale egenskaper tilbruk for klassifering er ekstrahert fra mikro-Doppler signalet, dette er; i) gjennomsnittlig radial hastighet, ii) grunnleggende gange frekvens, og iii) skittlengde.

Resultatene viser at ved å bruke disse parametrene kan man skille mellom menneske og hund. En egenskap som skiller de to type er at en hund har kortere ben og dermed en høyere gange frekvens og lavere skrittende ved samme radial hastighet, sammen liknet med et menneske.

Det er usikkert om dette er godt nok for et robust alarm/overvåkingssystem, bla fordi man kan tenke seg at en inntrenger kan "lure" systemet ved å bevege seg med feks korte skritt.

I tillegg viste det seg at egenskapene er følsomme for store endringer i radial hastighet. Dette kan sannsynligvis motvirkes ved en preprosessering før egenskapene bestemmes.

Hovedkonklusjoner er at på grunnlag av omfattende målinger av signaturer, ca 50 måleserien og omfattende beregninger og kombinasjone av de tre sentrale egenskap, har kommet frem til en av de mest robuste metodene for å skille mellom de to type mål man har sett på i oppgaven.

# Preface

This thesis was suggested and developed with the help of Novelda AS. It is a growing R&D based technology company based in Norway. Specializing in nanoscale wireless low-power technology for ultra-high resolution impulse radar. They have developed a flexible Ultra Wide Band (UWB) radar that can be used for a broad range of applications. One of the areas of interest is using the radar to automatically classify targets. Specifically on the subject of a home alarm system it is vital that the alarm is only triggered by a human and *not* animals (pets). To build a complete radar classifier for human and every type of pet is a tall order for a one man thesis. It was therefore decided to limit the scope of the thesis to only humans and dogs and not implement the classifier itself which is quite a large subject of its own. In addition it was decided to use the micro-Doppler signature to separate human and animals.

# Acknowledgment

I would like to thank Jan Roar Pleym, from Novelda AS, who suggested the subject of this thesis and gave good advice throughout. Also I would like to thank my thesis supervisor Lars Lundheim, from the Norwegian University of Science and Technology (NTNU), for assistance and inspiration.

A handwritten signature in black ink, reading "Thor Ø. Fossum". The signature is written in a cursive style with a large initial 'T' and a stylized 'Ø'.

Thor Øyvind Fossum

*Trondheim, July 3, 2015*

# Contents

<b>Abstract</b>	<b>I</b>
<b>Sammendrag</b>	<b>II</b>
<b>Preface</b>	<b>III</b>
<b>Acknowledgement</b>	<b>IV</b>
<b>1 Introduction</b>	<b>1</b>
1.1 Problem description . . . . .	1
1.1.1 Motivation and tasks . . . . .	2
1.1.2 The micro-Doppler signature . . . . .	2
1.1.3 Draft of a possible solution . . . . .	3
1.2 Outline of thesis . . . . .	4
<b>2 System Description</b>	<b>5</b>
2.1 System Overview . . . . .	5
2.2 Radar . . . . .	7
2.3 Time-Frequency Transforms . . . . .	12
2.3.1 Frame Buffer . . . . .	12
2.3.2 The Doppler Spectrum & the Range-Doppler Map . . . . .	13
2.3.3 Clutter Removal & $ \text{FFT} ^2$ . . . . .	18
2.3.4 Parameter estimation (RELAX) . . . . .	20
2.4 Extract $\mu$ -Doppler signature . . . . .	24
2.4.1 Tracking & range gate . . . . .	25
2.4.2 Synthesize $\mu$ -Doppler signature . . . . .	28
2.5 Gait-Doppler Map (feature extraction) . . . . .	30
<b>3 Results &amp; discussion</b>	<b>31</b>
3.1 Test setup . . . . .	31
3.2 Micro-Doppler signatures . . . . .	32

3.2.1	Human Signature & the Effects of Window Length . . . . .	32
3.2.2	Dog signature . . . . .	41
3.3	Gait-Doppler Map & features . . . . .	47
3.3.1	Gait-Doppler Map from Human . . . . .	47
3.3.2	Gait-Doppler Map from Dog . . . . .	50
3.3.3	Challenges . . . . .	53
<b>4</b>	<b>Concluding remarks</b>	<b>54</b>
4.1	Further work . . . . .	54
4.2	Conclusion . . . . .	55
	<b>Bibliography</b>	<b>57</b>
	<b>Appendices</b>	<b>58</b>
<b>A</b>	<b>Selected Matlab code</b>	<b>59</b>
A.1	The RELAX algorithm . . . . .	59

# Introduction

The basic radar concept was first demonstrated by experiments done by Heinrich Hertz from 1885 to 1888 and has more or less been continually improved upon since then. It was during the second world war however that the radar truly became ubiquitous and a vital part of a nations defense system. Still, it was after the war that the radar became more than a “blob” detector. [9, p.14-p.19].

The introduction of relative low-cost digital processing in the 70s meant that the pulse-Doppler approach that could measure target velocity and detect motion became dominant, having been held back by hardware limitations and cost. This allowed techniques like synthetic aperture radar (SAR) that previously had performance issues. The 70s is also the decade ultra wide band (UWB) started being used in commercial applications. [10][1]

A broad and interesting area is that of using the radar to classify radar targets so called automatic target recognition (ATR). Which is this thesis area of interest. Attempts at ATR has been made for a long time in radar. The earliest attempts seems to have been in 1937 with adding resonant dipole antennas to friendly planes to distinguish them from enemy aircraft. Such systems was of limited use especially when flying in formation. Other systems were later used but they relied upon the target cooperating (having transponders on targets) a so called “co-operative target”. Identifying a “non co-opertive target ” both for convenience or necessity, must most of the time be identified solely on the basis of the backscattered radar signal without reliance on external inputs. [10]

## 1.1 Problem description

This thesis concerns itself with the classification of humans and dogs by using the micro-Doppler signature.

### 1.1.1 Motivation and tasks

The classification of different animals is of great interest for example in a home alarm system. The radar will monitor a area and start an alarm if unwanted people (targets) are detected there. However one would not want to trigger the alarm for targets that are welcome like pets. In Skolniks *Introduction To Radar System*[9] there are nine radar techniques/phenomena identified that may be used for ATR, like High Range Resolution (HRR) or Radar Cross Section (RCS) fluctuation. All the phenomena are well understood but there is still areas of active research since the practical implementation of ATR is challenging. Instead of using all available techniques it was decided to focus on a technique that was broadly applicable to all kinds animals and explore how the radar performed and identify challenges. The technique chosen and explored in this thesis is what Skolnik called Jet Engine Modulation (JEM) which after continued research is now known as the more general micro-Doppler signature.

### 1.1.2 The micro-Doppler signature

A pulse radar measures the distance to target by emitting a signal and waiting for its echo from a target. Based on the time delay of the received signal the radar can measure the range of an object. If the target is moving the frequency of the received signal will be shifted from the emitted signal, this is known as the Doppler effect. The Doppler frequency is determined by the radial velocity of the target. The micro-Doppler effect is the intricate frequency modulations that are induced by the returns from the different moving components associated with the target that do not necessarily move with with the exact same radial speed as the bulk motion of the target (micro motions). Examples of such a component can be a moving limb on a animal, a propeller on a plane or the vibrations of its engine. The superposition of all these frequency modulation represented in the joint time and Doppler frequency domain is the micro-Doppler signature. It is labeled a signature since it is often distinct and can be used to differentiate and characterize targets. [3][10]

### 1.1.3 Draft of a possible solution

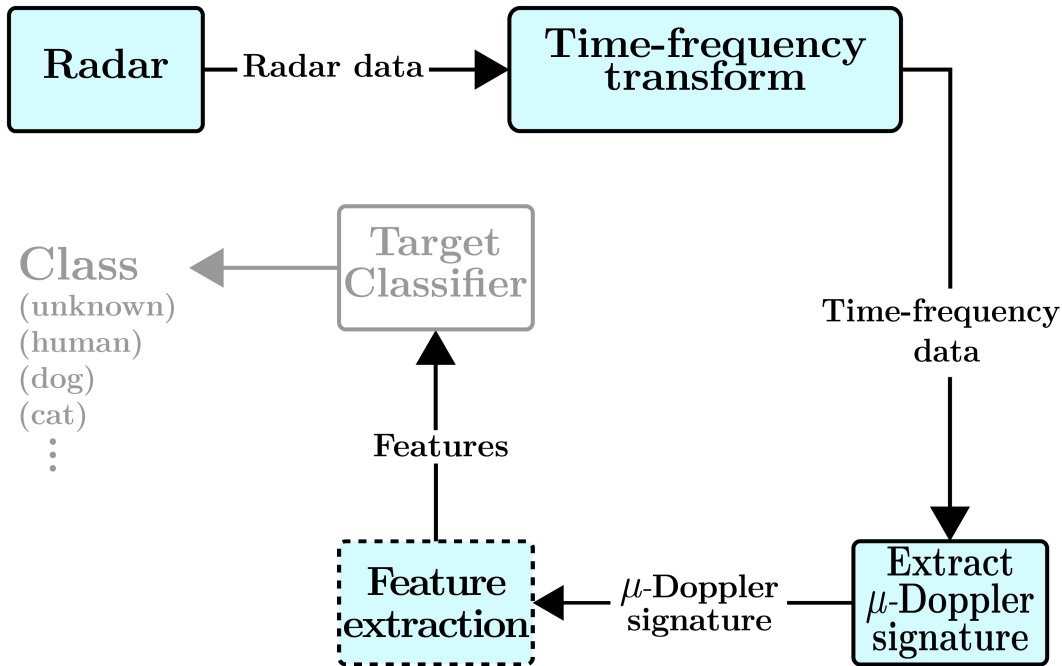


Figure 1.1: Draft of a possible solution to separate between human & animals

Figure 1.1 shows a possible solution to the problem of how a UWB radar can determine if a target is a human or a animal. Each step (boxes) performs a vital signal processing step that leads to classifying a radar target as a type of animal or unknown. It all starts in the *Radar* where the radar echo (data) is collected and sent to the *Time-Frequency transform* where time and Doppler frequency data of the radar echo is produced. Based on this data the *Extract  $\mu$ -Doppler signature* step produces the micro-Doppler signature. Based on the micro-Doppler signature the *feature extraction* step attempts to take out characteristic information from the signature and pass it to the classifier. The features are passed on to the *Target classifier* that makes a decision based on the features what class should be assigned to the target. Modern classifiers are usually trained with a large amount of data so they can learn the best way to decide what class is appropriate. It could be conceivable to pass the whole micro-Doppler signature to the *Target classifier* and let it do the work and skip extracting features. This is probably not a good idea as a few dominant characteristic properties of the signature would dominate the classifier and the result would be poorer [10].

As mentioned the classifier will not be implemented or further discussed in this thesis. The *Radar*, *Time-frequency transform* and *Extract  $\mu$ -Doppler signature* step will be discussed in detail in the next chapter. Some features will be extracted from the micro-Doppler signature but they will be treated less rigorously theoretically so the *Feature extraction* step will be discussed less formally. It is the micro-Doppler signature that is the main focus of this thesis.

## 1.2 Outline of thesis

Here a short overview of the chapters of the thesis is provided.

**1 Introduction** The subject of the thesis is introduced with a short historical account of radar and the problem and motivation behind it is described.

**2 System Description** The overall system and signal processing used to create the micro-Doppler signatures is described and necessary theory provided.

**3 Results & Discussion** How the system was tested and the most relevant results is presented. The results are discussed with the relevant results on the following pages.

**4 Concluding Remarks** Some suggestions on the further work that could be done is discussed and the thesis is concluded.

**A Selected Matlab Code** Some of the Matlab code used in the thesis is provided.

## System Description

To create a good micro-Doppler signature the data received from the radar must be processed heavily. In this chapter a conceptual description of this processing will be presented and subsequently examined in detail.

### 2.1 System Overview

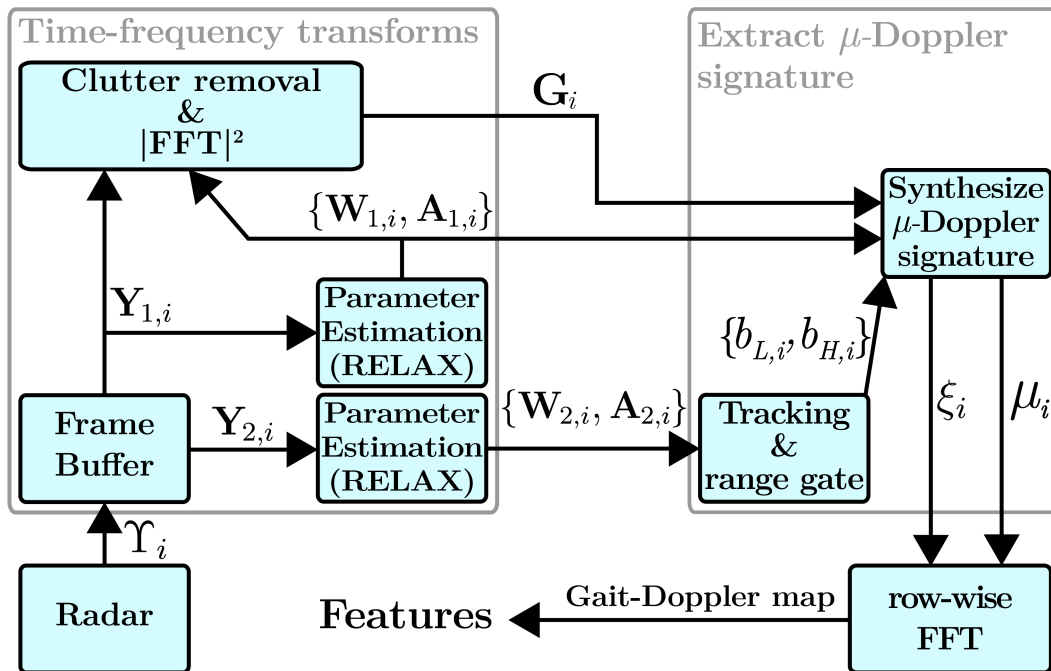


Figure 2.1: Conceptual overview of the system

Figure 2.1 shows a conceptual overview of how the signal received from the radar is processed. Each box in the figure is a high level representation of a important signal processing step. The radar box is of course also a sensor that is measuring the real world. Apart from the radar all the boxes has at least one input and one output which will be defined and described in the following sections.

It all begins with the *radar* that produces frames  $\Upsilon_i$  that the *Frame buffer* assembles into two matrices of frames  $\mathbf{Y}_{1,i}$  and  $\mathbf{Y}_{2,i}$ . The first matrix  $\mathbf{Y}_{1,i}$  is sent to the *Parameter estimation* and *Clutter removal*  $\mathcal{E} |FFT|^2$ . The *Clutter removal*  $\mathcal{E} |FFT|^2$  step outputs the range-Doppler map matrix  $\mathbf{G}_i$ . The range-Doppler map has had its clutter removed with the help of the set of parameters  $\{\mathbf{W}_{1,i}, \mathbf{A}_{1,i}\}$  that the *Parameter estimation* has estimated based on  $\mathbf{Y}_{1,i}$ . These parameters is along with the range-Doppler map sent to the *Synthesize  $\mu$ -Doppler signature* step where two micro-Doppler signatures are produced. The difference between the two signatures is that they rely on different time-frequency transforms. The micro-Doppler signature  $\mu_i$  uses the data in the range-Doppler map  $\mathbf{G}_i$  which is based on the Short Time Frequency Transform (STFT). The more experimental micro-Doppler signature  $\xi_i$  is based on the parameters  $\{\mathbf{W}_{1,i}, \mathbf{A}_{1,i}\}$  which are estimated by the RELAX algorithm (called parameter estimation in the figure) which is a time frequency transform that completely parameterize the data.

Both signatures are only interested in information from the ranges where the target is currently present. This is where the range gate defined by its lower bound  $b_{L,i}$  and its higher bound  $b_{H,i}$  is used. The bounds are created by the *Tracking*  $\mathcal{E}$  *range gate* step which rely on the parameters  $\{\mathbf{W}_{1,i}, \mathbf{A}_{1,i}\}$  estimated by the *Parameter Estimation* step that has  $\mathbf{Y}_{2,i}$  as its input.

The signatures are sent to the *row-wise FFT* step where the gait-Doppler map is created and from which some features can easily be determined.

## 2.2 Radar

A monostatic radar is a radar that has its transmitter and receiver located at the same place. A radar that has its transmitter and receiver separated in space is known as a bistatic radar, similarly a radar with several receivers located at different places is known as a multistatic radar. The radar used in this thesis is the Novelda Xethru UWB radar developed by Novelda AS in Norway. Although it technically has the transmitter and receiver separated they are so close that it is in practice a monostatic radar. Developed to be flexible and used in a range of tasks. It has been used to detect the presence of people, monitor respiration, tracking and more. It uses little power and emits little power so it is safe to use on and near living things. The table 2.1 lists the most relevant information about this radar. UWB radars are probably more instructive to think about in terms of their ultrashort in time pulses despite of the ultra wideband label. It's the spatially short pulses that usually are smaller than the length of most targets that distinguish the UWB radars not the fact that they are wideband (of course the wideband in frequency is a direct result of the short in time pulses). That the UWB pulse is shorter than the length of the target means that the target will decompose into its individual scattering components known as point scatterers [1].

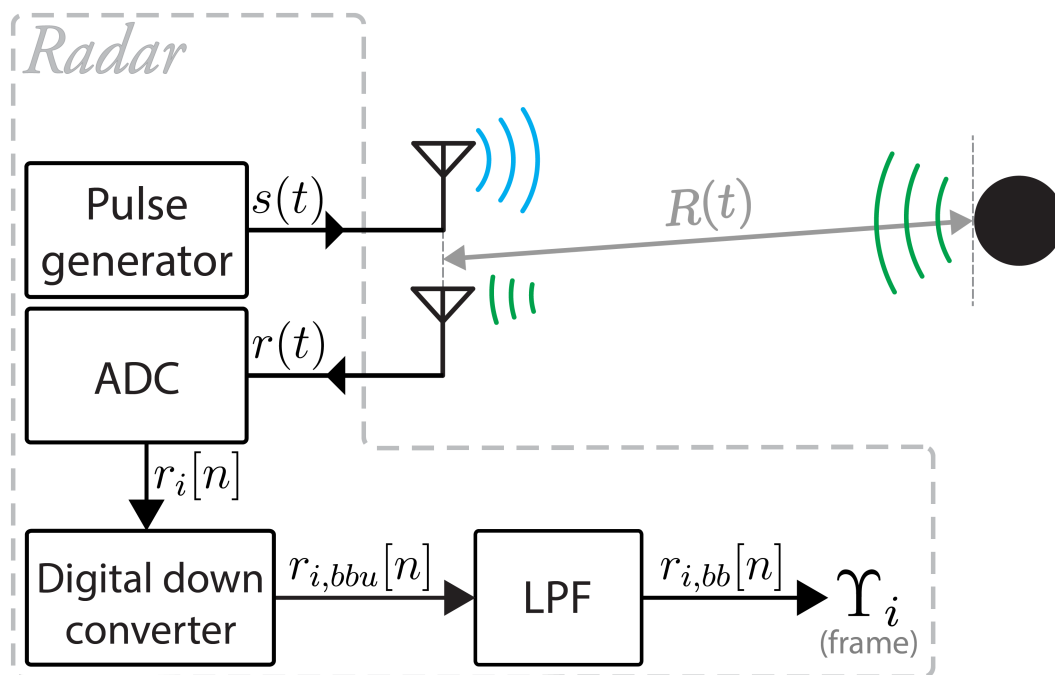


Figure 2.2: Conceptual overview of the radar with only one point scatterer ( $L = 1$ )

The target (human or dog) along with the environment that the radar detects will be modeled as a collection of point scatterers. Without loss of generality the theory can be developed with a single point scatterer since one can assume that the real target and the multipath interference is superposition of  $L$  point scatterers. A simplified overview of the radar used in this project is shown in figure 2.2. The model consists of a pulse

Table 2.1: Radar configuration

Carrier frequency ( $f_c$ )	$\sim 7$ GHz
Wavelength ( $\lambda$ )	$\sim 4.35$ cm
Pulse repetition frequency ( $f_p$ )	70 Hz
Samples per frame ( $N$ )	77
Frame span length	$\sim 2.7$ m

radar that emits a pulse  $s(t)$ , captures the echo contained in  $r(t)$  from a single point scatterer and downconverts it to baseband for further processing. The distance (range) between the radar and the point scatterer is denoted  $R(t)$ .

Unlike most radars that downconverts the carrier in the analog domain, the Xethru radar does this in the digital domain as outlined in figure 2.2. Using a ADC with a extremely high sampling frequency the radar digitizes  $r(t)$  directly. The radar does not samples  $r(t)$  all the time however and will digitize only a portion of  $r(t)$  after a pulse is emitted. This digital portion of  $r(t)$  is called a frame. The radar captures  $N = 77$  samples for every frame. The frame spans approximately 2.7 meters in space and its distance from the radar (frame offset) can be adjusted so that the frame span covers the desired target. This concept is illustrated in figure 2.3.

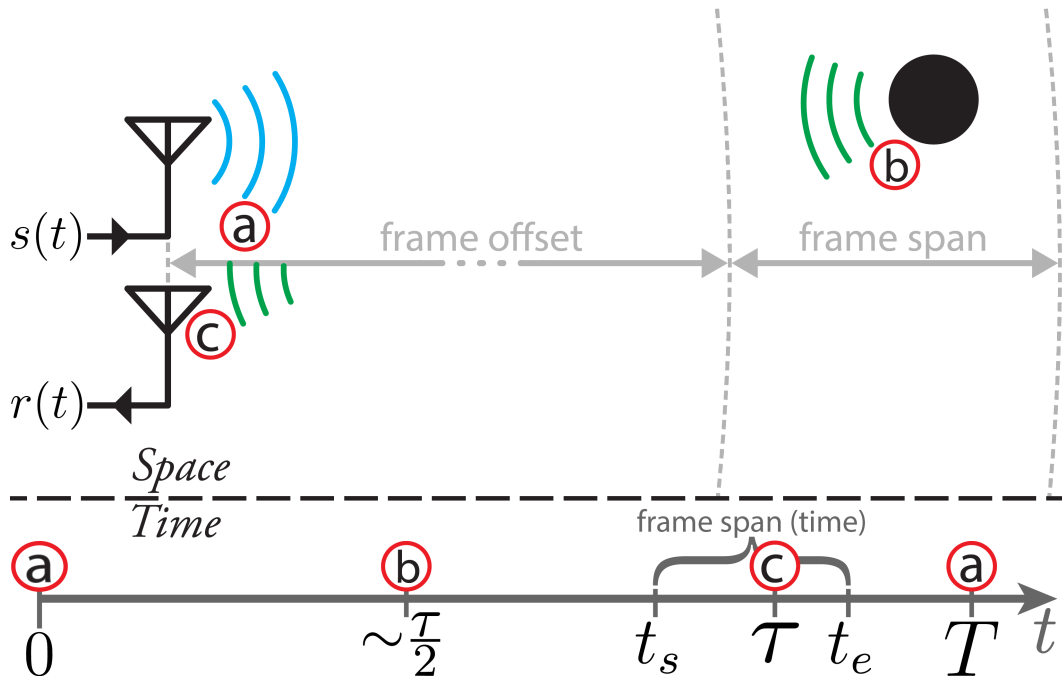


Figure 2.3: Frame offset and frame span illustrated, with a time line detailing when and where events happen.

Figure 2.3 illustrates the first cycle of emitting a pulse and recording its echo into a frame. The three main events of the emitted pulse is assigned letters (a,b and c) in the figure to make it easier to see where and when these events occurs. At (a) when

$t = 0$ , the radar begins emitting the first pulse. Then, at **(b)** when  $t \approx \frac{\tau}{2}$ , the pulse is reflected off the target (black circle), where  $\tau = \frac{2R(t)}{c}$ . Later, when  $t = t_s$  the radar starts recording (sampling)  $r(t)$  until the time  $t = t_e$ . At **(c)** when  $t = \tau$  the pulse is appearing in the receiver. Therefore  $t_s < \tau < t_e$  must be true if the pulse is going to be sampled and be a part of the frame.  $T$  is the pulse repetition period so when  $t = T$ , the second pulse starts emitting, beginning the cycle again. This means that,  $T = \frac{1}{f_p}$  where  $f_p$  is the pulse repetition frequency. For every pulse emitted one frame is produced.

The analog signal  $s(t)$  being sent out of the pulse generator, is defined as the sum of all pulses sent out, mathematically defined as

$$s(t) = \sum_{i=0}^{\infty} p(t - iT) \cos(\omega_c(t - iT)), \quad i = 0, 1, 2, \dots \infty \quad (2.1)$$

Where  $\omega_c$  is the angular carrier frequency which is defined as  $\omega_c = 2\pi f_c$  where  $f_c$  is the carrier frequency used by the radar. The function  $p$  represent a Gaussian pulse which is defined as

$$p(t) = \exp\left(-\frac{(t - \frac{T_p}{2})^2}{(2\sigma)^2}\right) \quad (2.2)$$

Typical values for  $\sigma$  and pulse duration  $T_p$  are 0.2 ns and 1 ns respectively. Figure 2.4 is a plot of such a pulse.

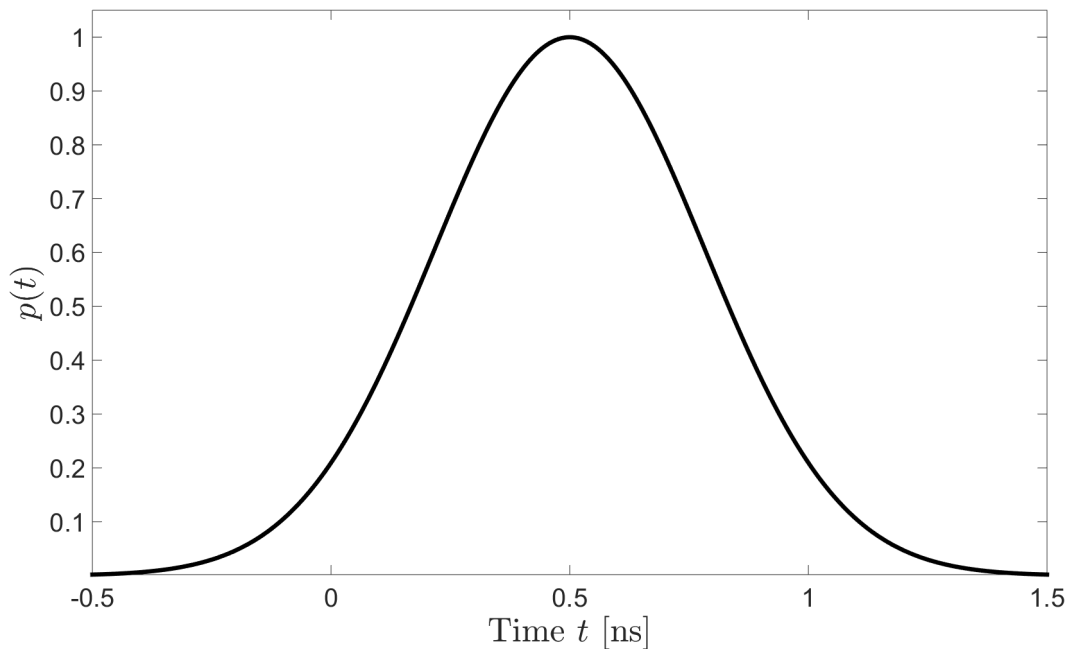


Figure 2.4: Gaussian pulse used in the UWB radar.

We define  $t_d$  as the time variable within the time interval  $(0, T)$ . Then the global time  $t$  can be written as

$$t = t_d + iT \quad (2.3)$$

With this definition of  $t$  it is easy to separate individual pulses (and therefore frames) with the variable  $i$ . It follows that  $t_d = t - iT$  as long as  $0 < t_d < T$ . This means that the  $i$ th sent pulse is

$$s_i(t_d) = p(t_d) \cos(\omega_c t_d) \quad (2.4)$$

When disregarding the attenuation, distortion and noise, the  $i$ th pulse being received by the antenna is the same signal as was sent, but now with a time delay  $\tau$ .

$$r_i(t_d) = s_i(t_d - \tau) = p(t_d - \tau) \cos(\omega_c(t_d - \tau)) \quad (2.5)$$

Where  $\tau$  is given as

$$\tau = \frac{2R(t)}{c} = \frac{2R(t_d + iT)}{c} \quad (2.6)$$

Substituting equation 3.1 into equation 2.5 results in

$$r_i(t_d) = p\left(t_d - \frac{2R(t_d + iT)}{c}\right) \cos\left(\omega_c\left(t_d - \frac{2R(t_d + iT)}{c}\right)\right) \quad (2.7)$$

Conversion of the signal from equation 2.7 into a frame, is done in the ADC shown in fig 2.2 but only when  $t_s < t_d < t_e$ . Mathematically we do this by substituting  $t_d = t_s + \Delta t n$  where  $\Delta t$  is the sampling period and

$$n = 0, 1, 2, \dots, N - 1 \quad (2.8)$$

Where  $N$  is the number of samples in the frame.  $t_s$  is, as illustrated in figure 2.3, the time offset determining the distance from the radar to the frame span. The time instant  $t_e$  can be expressed as  $t_e = t_s + \Delta t(N - 1)$ . Substituting  $t_d$  yields

$$\begin{aligned} r_i[n] &= r_i(t_s + \Delta t n) \\ &= p\left(t_s + \Delta t n - \frac{2R(t_s + \Delta t n + iT)}{c}\right) \\ &\quad \times \cos\left(\omega_c\left(t_s + \Delta t n - \frac{2R(t_s + \Delta t n + iT)}{c}\right)\right) \end{aligned} \quad (2.9)$$

Since we are observing humans and animals that move a extremely short distance during the time the frame is recorded (about 9 nanoseconds) we can make the following simplification.

$$R(t_s + \Delta t n + iT) \approx R(iT) \quad (2.10)$$

We can now write equation 2.9 as

$$r_i[n] \approx p\left(t_s + \Delta t n - \frac{2R(iT)}{c}\right) \cos\left(\omega_c\left(t_s + \Delta t n - \frac{2R(iT)}{c}\right)\right) \quad (2.11)$$

Next, the signal needs to be downconverted to baseband. As shown in figure 2.2 the received signal is sent to the digital downconverter. The downconversion is performed

by simply multiplying equation 2.11 and the complex sinusoid  $\exp(-j\omega_c(t_s + \Delta tn))$ .

$$\begin{aligned} r_{i,bbu}[n] &= r_i[n] \times \exp(-j\omega_c(t_s + \Delta tn)) \\ &= \frac{1}{2} \times p\left(t_s + \Delta tn - \frac{2R(iT)}{c}\right) \\ &\quad \times \left[ \exp\left(\frac{-j2\omega_c R(iT)}{c}\right) + \exp\left(-j2\omega_c\left(t_s + \Delta tn + \frac{R(iT)}{c}\right)\right) \right] \end{aligned} \quad (2.12)$$

$r_{i,bbu}$  goes through to low pass filter and removes the unnecessary last term of equation 2.12 and normalises it so we have

$$r_{i,bb}[n] = p\left(t_s + \Delta tn - \frac{2R(iT)}{c}\right) \exp\left(\frac{-j2\omega_c R(iT)}{c}\right) \quad (2.13)$$

Let  $\lambda = \frac{c}{f_c}$  where  $\lambda$  is the wavelength. Using this definition we express 2.13 with the wavelength instead of the carrier frequency.

$$r_{i,bb}[n] = p\left(t_s + \Delta tn - \frac{2R(iT)}{c}\right) \exp\left(\frac{-j4\pi R(iT)}{\lambda}\right) \quad (2.14)$$

Equation 2.14 shows that the contribution from a point scatterer to the frame is simply a amplitude provided from the Gaussian pulse and a phase from the remaining exponential function, in other words a phasor. It is the phase of the phasor that determines the Doppler shift. Let the phase be denoted  $\phi_i$  and defined as

$$\phi_i = \frac{-4\pi R(iT)}{\lambda} \quad (2.15)$$

The rate of change of  $\phi_i$  is the angular Doppler frequency  $\omega_d = 2\pi f_d$  where  $f_d$  is the Doppler frequency. We have

$$\omega_d = \frac{d\phi_i}{dt} = \frac{-4\pi}{\lambda} \frac{dR(iT)}{dt} = \frac{-4\pi v_r}{\lambda} \quad (2.16)$$

Where  $v_r = \frac{dR(iT)}{dt}$  is the radial velocity. The real targets (humans and animals) can as mentioned be modeled as a group of point scatterers. We therefore assume that the target and clutter can be modeled with  $L$  point scatterers, and so the  $i$ th frame denoted as  $\Upsilon_i[n]$  is expressed as

$$\Upsilon_i[n] = \sum_{l=0}^{L-1} p\left(t_s + \Delta tn - \frac{2R_l(iT)}{c}\right) \times \exp\left(\frac{-j4\pi R_l(iT)}{\lambda}\right) + v_i[n] \quad (2.17)$$

Where  $R_l(iT)$  is the range of the  $l$ th point scatterer and  $v_i$  is a vector containing the noise for the  $i$ th frame. Note that  $\Upsilon_i[n] = r_{i,bb}[n]$  only when  $L = 1$  if we ignore the noise term.

## 2.3 Time-Frequency Transforms

In general time-frequency analysis attempts to represent and manipulate a signal in time and frequency simultaneously. This is useful when observing signal whose frequency content changes over time, like music, speech, and the micro-Doppler signature from animal movements. Time-frequency analysis can therefore be thought of as a generalization of Fourier analysis which is most useful when the signal in question is stationary [4, p. 25]. There is a body of different techniques and methods to decompose a signal in both time and frequency. In this thesis two different time-frequency transforms is explored. The first is the well known short time Fourier transform (STFT) and the second is a parameter estimation performed with a algorithm known as RELAX [6]. Both methods work by having a sliding window extract a portion (in time) of the signal(s) and calculate the spectral contents of that portion. In this system two different window lengths are used, one for creating the range-Doppler map (more on that later) and one to track the desired target. First in this section the *frame buffer* that decides the window lengths is presented. Secondly what that information is contained in the windows is discussed in the subsection *The Doppler Spectrum & range-Doppler map*. After that the next subsection details the processing done in the *Clutter removal* step and the *Calculate spectrogram* step.

### 2.3.1 Frame Buffer

Note that from this point on, we denote matrices as boldface uppercase letters. The frame buffer takes several consecutive frames and groups them together into two different matrices denoted  $\mathbf{Y}_{1,i}$  and  $\mathbf{Y}_{2,i}$ .  $\mathbf{Y}_{1,i}$  has  $M_1$  consecutive frames in each column with the center column containing  $\Upsilon_i[n]$ . Similarly  $\mathbf{Y}_{2,i}$  has  $M_2$  consecutive frames in each column with the center column containing  $\Upsilon_i[n]$ . Since the only difference between the two matrices is the number of frames each contain both can be defined by the general matrix

$$\mathbf{Y}_{q,i} = \begin{bmatrix} y_{0,0} & y_{0,1} & \cdots & y_{0,M_q-1} \\ y_{1,0} & y_{1,1} & \cdots & y_{1,M_q-1} \\ \vdots & \vdots & \ddots & \vdots \\ y_{N-1,0} & y_{N-1,1} & \cdots & y_{N-1,M_q-1} \end{bmatrix}, \quad q = 1, 2 \quad (2.18)$$

where

$$y_{n,m} = \Upsilon_{i-\beta+m}[n], \quad m = 0, 1, \dots, M_q - 1 \quad (2.19)$$

and

$$\beta = \left\lfloor \frac{M_q}{2} \right\rfloor \quad (2.20)$$

The reason  $\mathbf{Y}_{1,i}$  and  $\mathbf{Y}_{2,i}$  use a different number of frames is that they are used for different purposes. The matrix  $\mathbf{Y}_{2,i}$  is used as the basis for tracking the desired target.



We assume that the window length  $M_q$  is so short that we can assume that no point scatterer is changing its radial speed  $v_{r,l}$ . This gives

$$R_l((i - \beta + m)T) \approx R_{l,i} + v_{r,l}mT \quad (2.23)$$

where

$$R_{l,i} = R_l(i - \beta) \quad (2.24)$$

Also assume that the amplitude of the point scatterers (in the specific range bin) is non-changing for the window duration.

$$p\left(t_s + \Delta tn - \frac{2R_l((i - \beta + m)T)}{c}\right) \approx \rho_{n,l} \quad (2.25)$$

We can now write  $y_n[m]$  as

$$y_n[m] \approx \sum_{l=0}^{L-1} \rho_{n,l} \exp\left(\frac{-j4\pi(R_{l,i} + v_{r,l}mT)}{\lambda}\right) + v_n[m] \quad (2.26)$$

Where we have added back a noise term with the same statistics as the one in equation 2.17. The equation above can be expressed as

$$y_n[m] = \sum_{l=0}^{L-1} \tilde{\rho}_{n,l} \exp\left(\frac{j2\pi f_{d,l}m}{f_p}\right) + v_n[m] \quad (2.27)$$

where  $\tilde{\rho}_{n,l}$  and  $f_{d,l}$  is the complex amplitude and the Doppler frequency of the  $l$ th point scatterer respectively. They are defined as

$$\tilde{\rho}_{n,l} = \rho_{n,l} \exp\left(\frac{-j4\pi R_{l,i}}{\lambda}\right) \quad (2.28)$$

$$2\pi f_{d,l} = -\frac{4\pi v_{r,l}}{\lambda f_p} \quad (2.29)$$

As mentioned  $f_p = 1/T$  is the pulse repetition frequency. Since  $y_n[m]$  is a digital signal with  $f_p$  as its sampling frequency, it is simplest to express it with its normalized angular Doppler frequency  $\tilde{\omega}_d$  defined as

$$\tilde{\omega}_d = \frac{\omega_d}{f_p} = \frac{2\pi f_d}{f_p} \quad (2.30)$$

meaning that the normalized angular Doppler frequency of the  $l$ th point scatterer is

$$\tilde{\omega}_{d,l} = \frac{2\pi f_{d,l}}{f_p} \quad (2.31)$$

$y_n[m]$  then becomes

$$y_n[m] = \sum_{l=0}^{L-1} \tilde{\rho}_{n,l} \exp(j\tilde{\omega}_{d,l}m) + v_n[m] \quad (2.32)$$

Realistically most of the  $L$  point scatterers will have a amplitude  $\rho_{n,l}$  that is not large enough to be measured in noise in the specific range bin  $n$ . This is of course the point

of using a UWB radar that has a short (in time) pulse. It makes it possible to separate targets in range since the pulse they reflect appears and disappears relatively quickly. It is therefore more useful to think of the subset of the  $L$  point scatterers that is relevant in a specific range bin  $n$ . By relevant we mean the point scatterers that are observable in the current noise. On this basis we write equation 2.32 on the form

$$y_n[m] = \sum_{k=0}^{K-1} \alpha_{n,k} \exp(j\Omega_{n,k}m) + \tilde{v}_n[m] \quad (2.33)$$

Where  $\alpha_{n,k}$  and  $\Omega_{n,k}$  is the complex amplitude and the normalized angular Doppler frequency respectively of the  $k$ th point scatterer in the range bin  $n$  that is observable.  $y_n[m]$  is now expressed with the  $K \leq L$  point scatterers that is relevant at that range. Note that  $y_n[m]$  itself has not changed since the noise has changed to account for the small contributions from the remaining point scatterers. Since  $K$  can (and probably will) vary depending on the range bin  $n$  it should strictly speaking be denoted as a variable dependent on  $n$  like for example  $K_n$ . This not done however to reduce clutter in the notation, still the reader should keep this in mind. This relationship between  $L$  and  $K$  is illustrated in figure 2.8.

By calculating the magnitude of the DTFT of equation 2.33 we obtain the Doppler spectrum of range bin  $n$  centered at the time  $t = iT$ . By standard DTFT transform theory we see that if  $y_n[m]$  were infinitely long we would have

$$|Y_n(\tilde{\omega}_d)| = |DTFT\{y_n[m]\}| = \sum_{k=0}^{K-1} \alpha_{n,k} \delta(\tilde{\omega}_d - \Omega_{n,k}) + |DTFT\{\tilde{v}_n[m]\}| \quad (2.34)$$

Where  $\delta(\cdot)$  represent the Dirac delta function. Equation 2.34 shows that under its idealized conditions the amplitude response produced by the DTFT would represent the  $k$ th point scatterer as a peak with amplitude  $|\alpha_{n,k}|$  and located at  $\tilde{\omega}_d = \Omega_{n,k}$ . The peak will be visible if its amplitude is larger than the noise floor created by the last term of equation 2.34. In practice  $y_n[m]$  is limited to  $M_q$  samples so there would be leakage. Assuming a rectangular window of length  $M_q$  equation 2.34 becomes

$$|Y_n(\tilde{\omega}_d)| = \sum_{k=0}^{K-1} \alpha_{n,k} \left| \frac{\sin \left[ \left( \tilde{\omega}_d - \Omega_{n,k} \right) \frac{M_q}{2} \right]}{\sin \left[ \left( \tilde{\omega}_d - \Omega_{n,k} \right) \frac{1}{2} \right]} \right| + |DTFT\{\tilde{v}_n[m]\}| \quad (2.35)$$

Comparing equation 2.35 and 2.34 it is easy to see that the Dirac delta function has been replaced by a fraction of two sinusoids that closely resembles the sinc function. This means that peaks now have a main-lobe and side-lobes as illustrated by figure 2.6. The main-lobe has a bandwidth given by

$$\text{Main-lobe bandwidth} = \frac{f_p}{M_q} = \frac{1}{M_q T} \quad (2.36)$$

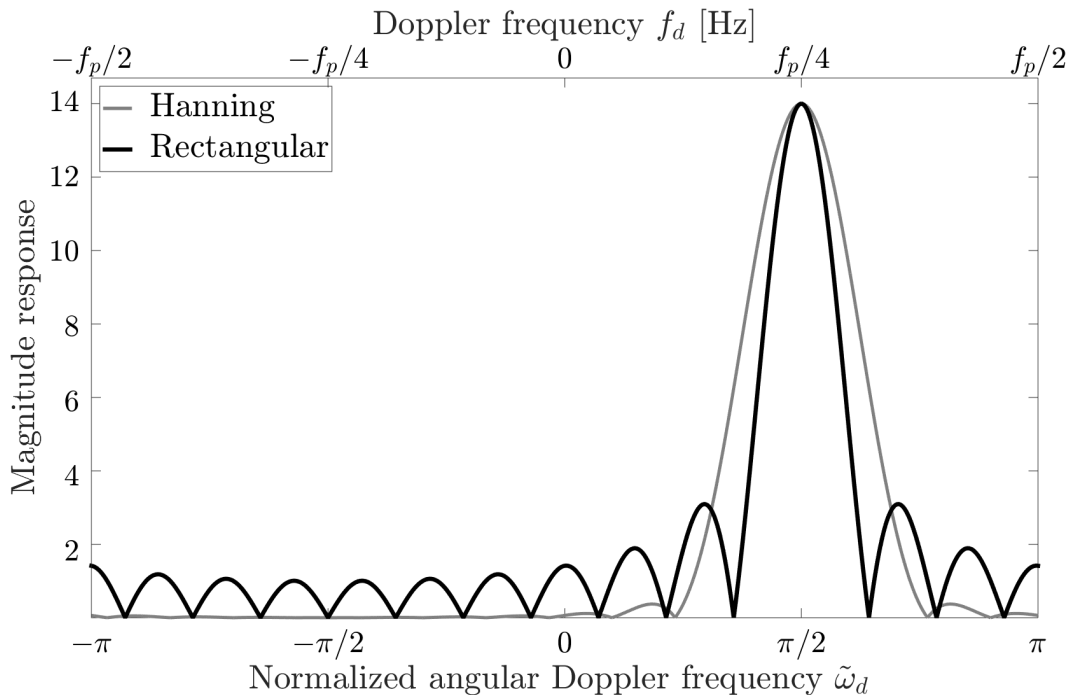


Figure 2.6: DTFT of a single point scatterer with constant radial speed so that  $f_d = f_p/4$  (black). Included is the DTFT with a Hanning window applied first to the same point scatterer (gray). The amplitude of the windowed DTFT has been corrected for amplitude loss. In both cases  $M_q = 14$ .

In practice when calculating the STFT a Hanning window is applied resulting in a wider main-lobe bandwidth but suppressed side-lobes (also illustrated in 2.6). The RELAX algorithm however (which is defined later in this text) and the mathematics in this section uses a rectangular windows. Equation 2.36 expresses the trade-off between time and frequency, that lies at the heart of all time frequency analysis. It clearly states that the main-lobes bandwidth is inversely proportional to the total time span of the signal. A smaller main-lobe meaning better frequency resolution requires that a bigger window in time (bigger  $M_q$ ). A bigger window in time means that the assumptions made from equation 2.23 to 2.25 becomes less accurate. The resolution in time (how accurate the spectrum reflects the situation at a specific instance) is reduced. Another effect of a bigger window is better signal to noise ratio. The reason is that the DTFT performs coherent radar pulse integration. In theory, coherent integration is lossless, meaning that the signal to noise ratio of  $M_q$  integrated pulses denoted  $\text{SNR}_{M_q}$  is exactly  $M_q$  times that of a single pulse denoted  $\text{SNR}_1$  [9, p.46]. Because of the early transition from the analog to the digital domain that the radar does it has very good coherence (phase accuracy). Therefore assuming  $\text{SNR}_{M_q} \approx M_q \times \text{SNR}_1$  should be a good assumption (at least for  $M_q < 30$ ). This is the motivation to use the matrix  $\mathbf{Y}_{2,i}$  which has more pulses (frames) included compared to  $\mathbf{Y}_{1,i}$  ( $M_2 > M_1$ ) for tracking. Having good enough signal to noise ratio to tracking is a prerequisite to create a good micro-Doppler signature and therefore worth the reduced time resolution.

The Doppler spectrum is as discussed a superposition of point scatterers and noise. The point scatterers represent echos from everything in the environment the radar observes. All the echos that is from the natural environment that is *unwanted* is known as clutter. Often non-moving and very slow moving objects will dominate the echos received and will be the biggest source of clutter. This means that if the desired targets are moving slow enough they have a great risk of being masked by the clutter. The figure 2.7 is an illustration of a plausible Doppler spectrum. A noise floor (white noise in the figure) means that only targets (point scatterers) reflecting enough power to be above the floor are observable. Clutter dominates around 0 Hertz in the spectrum. Two moving targets are observed, one moving away from the radar (outbound) and one moving towards the radar (inbound) twice as fast.

The reason a target can theoretically be observed without aliasing with a  $f_d$  right below  $f_p$  (as opposed to  $f_p/2$ ) is a result of knowing the targets direction (in relation to the radar). Given that we know the target's direction and no other targets or clutter is moving the opposite direction. If the direction is inbound the Doppler frequency is equal to or greater than 0Hz meaning that if the inequation chain  $0 \leq f_d < f_p$  is true there is no aliasing. Similarly a outbound direction means if  $0 \geq f_d > -f_p$  is true there is no aliasing.

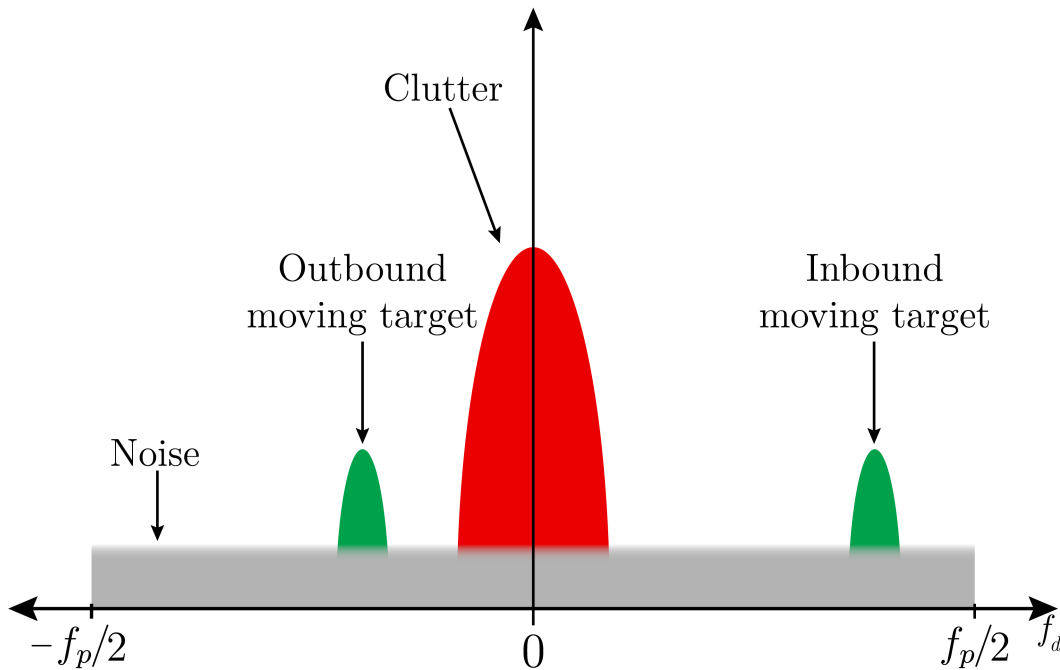


Figure 2.7: Illustration of a Doppler spectrum with two moving targets with clutter and noise. The inbound moving target is twice as fast compared to the outbound moving target

The range-Doppler map  $\mathbf{G}_i$  is simply a matrix consisting of the Doppler spectrums of all the individual radar ranges. As seen in figure 2.1 it is the output of the *Calculate spectrogram* step. It consists of all  $N$  Doppler spectrums obtained from  $\mathbf{Y}_{1,i}$ . Its formal

definition is in the next section below. To visualize the range-Doppler map observe figure 2.8 that illustrates a range-Doppler Map where  $N = 11$  and  $L = 24$  idealized point scatterers.

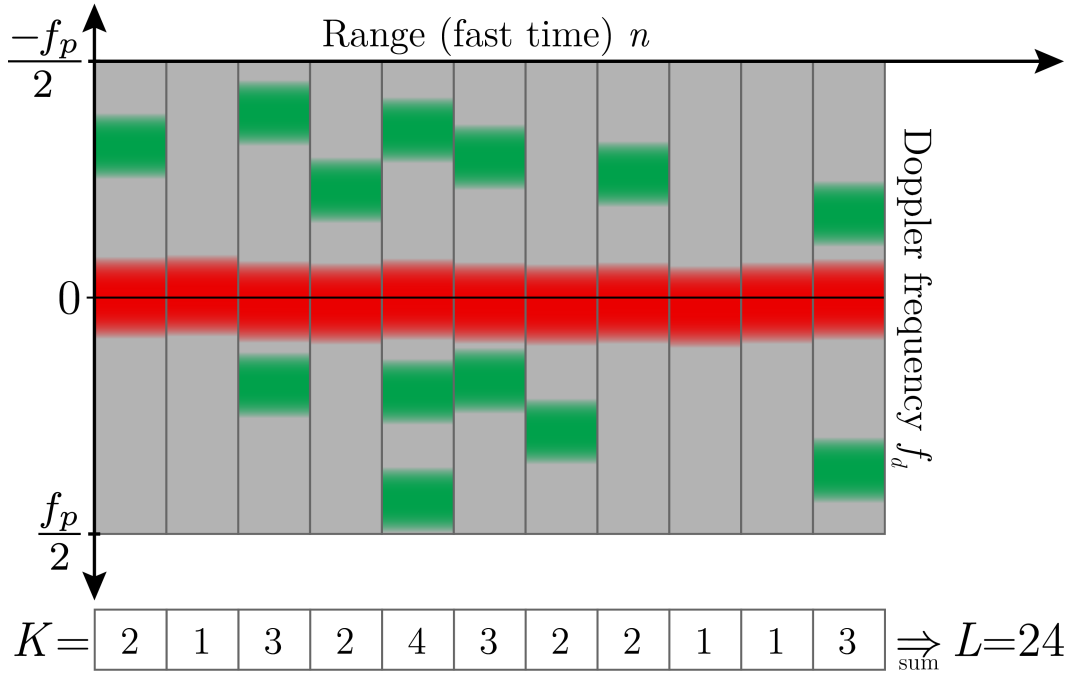


Figure 2.8: Illustration of a range Doppler map with a total of  $L = 24$  point scatterers and  $N = 11$

### 2.3.3 Clutter Removal & $|\text{FFT}|^2$

The clutter contain no information about our desired target and its DTFT leakage interferes with the spectrum. Removing the clutter is therefore a useful step to create a good micro-Doppler signature. Since the micro-Doppler signature is based on the range-Doppler map the clutter should be removed before the range-Doppler map is created. The details of how the clutter is removed is in the table 2.2 which details how the range-Doppler Map  $\mathbf{G}_i$  is calculated. It is built column by column by the row signal from  $\mathbf{Y}_{1,i}$  which we in this subsection temporarily denote as  $y_n[m]$  ( $y_n[m]$  was strictly speaking defined on the basis of  $\mathbf{Y}_{q,i}$  in the section above). It still has the same form

$$y_n[m] = \sum_{k=0}^{K-1} \alpha_{n,k} \exp(j\Omega_{n,k}m) + \tilde{v}_n[m], \quad m = 0, 1, 2, \dots, M_1 - 1 \quad (2.37)$$

To perform the clutter removal the matrices  $\{\mathbf{W}_{1,i}, \mathbf{A}_{1,i}\}$  from the *parameter estimation* step is used. The matrices are defined by the equations 2.50a and 2.50b. These matrices contain the  $K$  estimated angular frequencies  $\{\hat{\Omega}_{n,k}\}_{k=0}^{K-1}$  and complex amplitudes  $\{\hat{\alpha}_{n,k}\}_{k=0}^{K-1}$  for all  $N$  range bins. These parameters are used to remove the clutter in the the time domain before calculating the range-Doppler map. In this case clutter

is defined as having the absolute value of the estimated angular normalized frequency  $|\hat{\Omega}_{n,k}|$  less than a threshold  $\epsilon_f$ . After the clutter is removed a Hanning window is applied and the signal zero-padded to have a length of  $D$  which is the frequency sampling factor used in the fast Fourier transform (FFT). Consequently  $d = 0, 1, 2, \dots, D - 1$  is the discrete frequency index. The usual way of using a time-frequency representation from the STFT is with the spectrogram which is simply the squared of its magnitude response [5]. The spectrogram of the signal  $x$  for example is

$$\text{spectrogram}\{x\} = |\text{STFT}\{x\}|^2 \tag{2.38}$$

Remember that  $y_n[m]$  is the STFT signal portion (after clutter removal and zero-padding) in this case. The spectrogram convention is therefore followed by expressing range-Doppler map  $\mathbf{G}_i$  with the magnitude-squared of the FFT performed on the zero-padded signal (see table 2.2).

Table 2.2: Range-Doppler map creation (clutter removal &  $|\text{FFT}|^2$ )

---



---

**input**

$$\{\mathbf{W}_{1,i}, \mathbf{A}_{1,i}\} \Rightarrow \begin{cases} \{\hat{\alpha}_{n,k}\}_{k=0}^{K-1}, & n = 0, 1, \dots, N-1 \\ \{\hat{\Omega}_{n,k}\}_{k=0}^{K-1}, & n = 0, 1, \dots, N-1 \end{cases}$$

$$\mathbf{Y}_{1,i} \Rightarrow y_n[m], \quad m = 0, 1, \dots, M_1 - 1, \quad n = 0, 1, \dots, N-1$$

**initialize**

$w[m] = M_1$  samples long Hanning window

$y_p[d] = 0, \quad d = 0, 1, \dots, D-1$

**for**  $n = 0, 1, \dots, N-1$

$\tilde{y}[m] = y_n[m], \quad m = 0, 1, \dots, M_1 - 1$

**for**  $k = 0, 1, \dots, K-1$

**if**  $|\hat{\Omega}_{n,k}| < \epsilon_f$

$\tilde{y}[m] = \tilde{y}[m] - \hat{\alpha}_{n,k} \exp(j\hat{\Omega}_{n,k}m), \quad m = 0, 1, \dots, M_1 - 1$

**end if**

**end for**

$\tilde{y}[m] = \tilde{y}[m] \times w[m], \quad m = 0, 1, \dots, M_1 - 1$

$y_p[m] = \tilde{y}[m], \quad m = 0, 1, \dots, M_1 - 1$  (zero-padding)

$g_{n,d} = \frac{1}{M_1} \left| \sum_{s=0}^{D-1} y_p[m] \exp(-j2\pi d \frac{s}{D}) \right|^2, \quad d = 0, 1, \dots, D-1$

**end for**

**output**

$$\mathbf{G}_i = \begin{bmatrix} g_{0,0} & g_{0,1} & \cdots & g_{0,D-1} \\ g_{1,0} & g_{1,1} & \cdots & g_{1,D-1} \\ \vdots & \vdots & \ddots & \vdots \\ g_{N-1,0} & g_{N-1,1} & \cdots & g_{N-1,D-1} \end{bmatrix}$$


---



---

### 2.3.4 Parameter estimation (RELAX)

The parameter estimation is a way of getting a better trade off between time and frequency resolution compared to using the STFT. By performing a spectral analysis with a spectral estimation algorithm (also referred to as a super-resolution algorithm) the resolution in frequency and time can be improved [4, p.13]. The algorithm used is the RELAX algorithm proposed by Jian Li and Petre Stoica [6]. The algorithm is designed with feature extraction in radar applications in mind such as inverse synthetic aperture radar (ISAR) imaging. It is applied on the rows of  $\mathbf{Y}_{1,i}$  and  $\mathbf{Y}_{2,i}$ . It is used to estimate complex sinusoids in a noisy signal. We therefore make the same assumptions

made from equation 2.23 to 2.25. Then we can work on the signal from equation 2.33.

$$y_n[m] = \sum_{k=0}^{K-1} \alpha_{n,k} \exp(j\Omega_{n,k}m) + \tilde{v}_n[m] \quad (2.39)$$

The algorithm will be attempting to estimate the angular Doppler frequencies  $\Omega_{n,k}$  and the corresponding complex amplitudes  $\alpha_{n,k}$ . This equation expresses  $y_n[m]$  as the sum of the  $K$  point scatterers that are above the noise floor. How many that actually are is unfortunately unknown and varies depending on the range  $n$ . Instead of attempting to estimate how many there is, a constant  $K$  is assumed. By setting  $K$  high enough one ensures that no point scatterer is likely missed, this also implies that a number of non existing point scatterers is estimated but this is acceptable. Practical testing revealed that  $K = 8$  was enough to work well with one target. These parameters will be used to performing tracking and clutter rejection, in addition some experimentation of using it as a alternative to the STFT to create a micro-Doppler signature is investigated. As shown in figure 2.1 this parameter estimation is done on both matrices  $\mathbf{Y}_{1,i}$  and  $\mathbf{Y}_{2,i}$ . The results from  $\mathbf{Y}_{1,i}$  is the parameters used both for removing clutter and create a micro-Doppler signature. The parameters from  $\mathbf{Y}_{1,i}$  is used for the tracking and range gating of the target.

We recognize that equation 2.39 shows that the general form of the equation does not change with  $n$  (the range bin currently being processed). We therefore omit  $n$  to make the notation less cluttered when presenting the algorithm.

$$y[m] = \sum_{k=0}^{K-1} \alpha_k \exp(j\Omega_k m) + \tilde{v}[m] \quad (2.40)$$

Just as before we denote matrices as boldface uppercase letters, now in addition we denote vectors as boldface lowercase letters. Note that  $(\cdot)^T$  is the transpose,  $(\cdot)^H$  is the conjugate transpose and  $\|\cdot\|$  is the euclidean norm. We define the following vectors

$$\mathbf{a}(\Omega_k) = [1 \quad \exp(j1\Omega_k) \quad \exp(j2\Omega_k) \quad \cdots \quad \exp(j(M_q - 1)\Omega_k)]^T \quad (2.41)$$

$$\mathbf{v} = [\tilde{v}[0] \quad \tilde{v}[1] \quad \cdots \quad \tilde{v}[M_q - 1]]^T \quad (2.42)$$

$$\mathbf{y} = [y[0m] \quad y[1] \quad \cdots \quad y[M_q - 1]]^T \quad (2.43)$$

Using these equations, equation (2.40) can be written as

$$\mathbf{y} = \sum_{k=0}^{K-1} \alpha_k \mathbf{a}(\Omega_k) + \mathbf{v} \quad (2.44)$$

The maximum likelihood (ML) estimator given zero-mean white Gaussian noise requires solving the minimization problem [7]

$$\{\hat{\alpha}_k, \hat{\Omega}_k\}_{k=0}^{K-1} = \arg \min_{\{\alpha_k, \Omega_k\}_{k=0}^{K-1}} \left\| \mathbf{y} - \sum_{k=0}^{K-1} \alpha_k \mathbf{a}(\Omega_k) \right\|^2 \quad (2.45)$$

Which is a nonlinear least-squares fitting problem and can be solved efficiently with the RELAX algorithm. The algorithms pseudocode is outlined in table 2.3.

Table 2.3: RELAX Algorithm

---



---

```

initialize
 $\hat{\alpha}_k = 0, \quad k = 1, 2, \dots, K - 1$ 
( $\hat{\Omega}_k$  values are not needed to initialize)
for  $s = 0, 1, \dots, K - 1$ 
     $\hat{\mathbf{y}}_s = \mathbf{y} - \sum_{k=0, k \neq s}^{K-1} \hat{\alpha}_k \mathbf{a}(\hat{\Omega}_k)$ 
     $\hat{\Omega}_s = \arg \max_{\Omega} \frac{\|\mathbf{a}^H(\Omega) \hat{\mathbf{y}}_s\|^2}{\|\mathbf{a}(\Omega)\|^2}$ 
     $\hat{\alpha}_s = \frac{\mathbf{a}^H(\hat{\Omega}_s) \hat{\mathbf{y}}_s}{\|\mathbf{a}(\hat{\Omega}_s)\|^2}$ 
repeat
    for  $j = 0, 1, \dots, s$ 
         $\hat{\mathbf{y}}_j = \mathbf{y} - \sum_{m=1, m \neq j}^s \hat{\alpha}_m \mathbf{a}(\hat{\Omega}_m)$ 
         $\hat{\Omega}_j = \arg \max_{\Omega} \frac{\|\mathbf{a}^H(\Omega) \hat{\mathbf{y}}_j\|^2}{\|\mathbf{a}(\Omega)\|^2}$ 
         $\hat{\alpha}_j = \frac{\mathbf{a}^H(\hat{\Omega}_j) \hat{\mathbf{y}}_j}{\|\mathbf{a}(\hat{\Omega}_j)\|^2}$ 
    end for
until(convergence)
end for
    
```

---



---

One of the reasons the algorithm is efficient is because it relies on the periodogram (which uses the FFT) to estimate the angular frequency  $\Omega_k$ . The periodogram of  $y[m]$  is

$$P(\Omega) = \frac{1}{M_q} \left| \sum_{m=0}^{M_q-1} y[m] \exp(-j\Omega m) \right|^2 = \frac{\|\mathbf{a}^H(\Omega) \mathbf{y}\|^2}{M_q} \quad (2.46)$$

The signal should be zero-padded enough to achieve high accuracy when estimating frequency. The signals used in this thesis was zero-padded to a length of 2048 which is twice the length used in [6].

The minimization problem 2.45 is solved by successively solving the simpler problem

$$\{\hat{\alpha}_s, \hat{\Omega}_s\} = \arg \min_{\{\alpha_s, \Omega_s\}} \|\hat{\mathbf{y}}_s - \alpha_s \mathbf{a}(\Omega_s)\|^2 \quad (2.47)$$

Minimizing the right side of 2.47 with respect to  $\alpha_s$  gives us

$$\hat{\alpha}_s = \frac{\mathbf{a}^H(\hat{\Omega}_s)\hat{\mathbf{y}}_s}{\|\mathbf{a}(\hat{\Omega}_s)\|^2} \quad (2.48)$$

Substituting equation 2.48 into 2.47 results in

$$\hat{\Omega}_s = \arg \max_{\Omega_s} \frac{\|\mathbf{a}^H(\Omega_s)\hat{\mathbf{y}}_s\|^2}{\|\mathbf{a}(\Omega_s)\|^2} \quad (2.49)$$

Observe that  $\|\mathbf{a}(\Omega_s)\|^2 = M_q$  and that equation 2.49 is therefore equal to the periodogram of  $\hat{\mathbf{y}}_s$ . In this way the fft is used to estimate  $\hat{\Omega}_s$  by taking the location of the biggest peak in the periodogram of  $\hat{\mathbf{y}}_s$ . With the location of  $\hat{\mathbf{y}}_s$  the complex amplitude  $\hat{\alpha}_s$  can be easily found with the same fft.

To utilize these results to the fullest a relatively simple cyclic concept is used where the new parameters  $\{\hat{\alpha}_s, \hat{\Omega}_s\}$  are not estimated until  $\{\hat{\alpha}_s, \hat{\Omega}_s\}_{s=1}^{i-1}$  are “sufficiently good”. In other words, until the previous estimates converge. Convergence is determined by checking how much the cost function 2.45 changes between two successive iteration of the repeat-until-loop. When the difference is less than a predefined threshold  $\epsilon_c$  the estimates are said to have converged. The RELAX algorithm takes advantage of the fact that the calculation of the dominant peak in the periodogram is more accurate when it consists of a single sinusoid, instead of two or more sinusoids. This especially true if the sinusoids are closely spaced to eachother. This is a very attractive feature use since it is desirable to use a few samples (small  $M_q$ ) so one can have good time resolution, which result in a lot of leakage (low resolution) in the periodogram. This is mitigated however since  $\hat{\mathbf{y}}_s$  is assumed to eventually consist only of one complex sinusoid, the others and their interfering leakage removed.

The results of the RELAX algorithm is of the set of all  $K$  angular frequencies and complex amplitudes estimated at range  $n$  denoted  $\{\hat{\Omega}_{n,k}\}_{k=0}^{K-1}$  and  $\{\hat{\alpha}_{n,k}\}_{k=0}^{K-1}$ . The algorithm is applied to all ranges and the result is collected in two matrices  $\mathbf{W}_{q,i}$  and  $\mathbf{A}_{q,i}$  where just as before  $q = \{1, 2\}$  and denotes if the input was  $\mathbf{Y}_{1,i}$  or  $\mathbf{Y}_{2,i}$ . Given that  $\mathbf{Y}_{q,i}$  is the input to the parameter estimation and the parameters estimated at range  $n$  is  $\{\hat{\Omega}_{n,k}\}_{k=0}^{K-1}$  and  $\{\hat{\alpha}_{n,k}\}_{k=0}^{K-1}$ . The output of the parameter estimation is  $\{\mathbf{W}_{q,i}, \mathbf{A}_{q,i}\}$  defined as

$$\mathbf{W}_{q,i} = \begin{bmatrix} \hat{\Omega}_{0,0} & \hat{\Omega}_{0,1} & \cdots & \hat{\Omega}_{0,K-1} \\ \hat{\Omega}_{1,0} & \hat{\Omega}_{1,1} & \cdots & \hat{\Omega}_{1,K-1} \\ \vdots & \vdots & \ddots & \vdots \\ \hat{\Omega}_{N-1,0} & \hat{\Omega}_{N-1,1} & \cdots & \hat{\Omega}_{N-1,K-1} \end{bmatrix}, \quad q = 1, 2 \quad (2.50a)$$

and

$$\mathbf{A}_{q,i} = \begin{bmatrix} \hat{\alpha}_{0,0} & \hat{\alpha}_{0,1} & \cdots & \hat{\alpha}_{0,K-1} \\ \hat{\alpha}_{1,0} & \hat{\alpha}_{1,1} & \cdots & \hat{\alpha}_{1,K-1} \\ \vdots & \vdots & \ddots & \vdots \\ \hat{\alpha}_{N-1,0} & \hat{\alpha}_{N-1,1} & \cdots & \hat{\alpha}_{N-1,K-1} \end{bmatrix}, \quad q = 1, 2 \quad (2.50b)$$

## 2.4 Extract $\mu$ -Doppler signature

The micro-Doppler signature  $\mu_i$  is extracted from the range-Doppler map by summing together all the range bins that contain point scatterers from the desired target. Let the range bin *nearest* the radar containing point scatterers from the desired target at time  $t = iT$  be denoted  $b_{L,i}$ . Similarly let the range bin *furthest away* from the radar containing point scatterers from the desired target at time  $t = iT$  be denoted  $b_{H,i}$ .  $b_{L,i}$  and  $b_{H,i}$  define the lower bound and higher bound of the range gate respectively. Only the range bins inside the range gate will be added together and become a part of the micro-Doppler signature  $\mu_i$ . This is illustrated by figure 2.9 where the range bins inside the range gate of  $\mathbf{G}_i$  is colored red. They are added together and becomes the last entry (in the column dimension) of signature  $\mu_i$ .

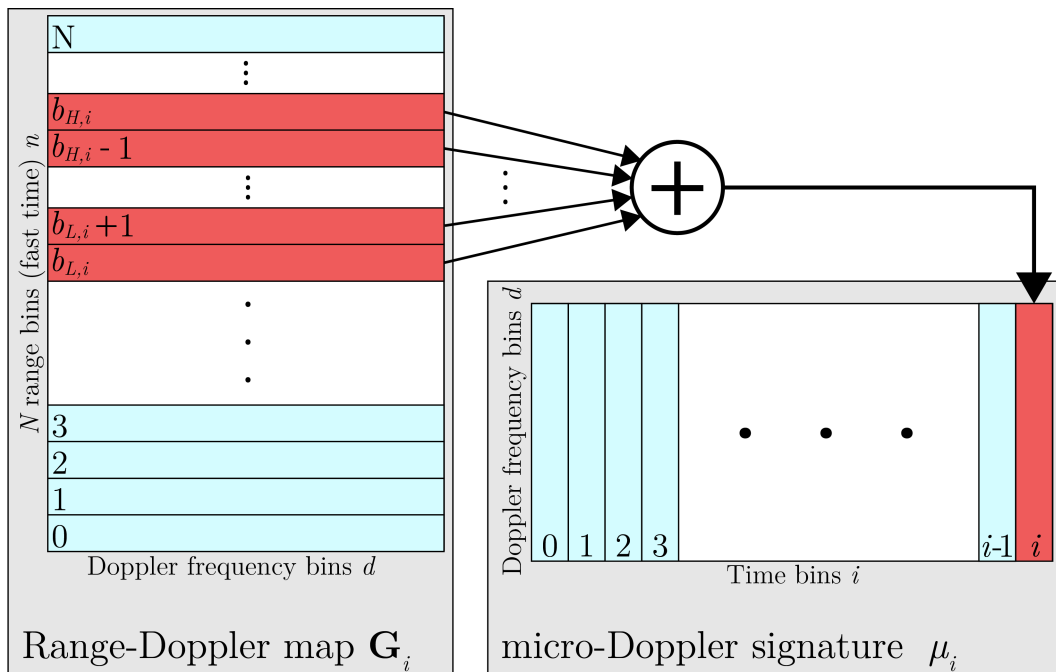


Figure 2.9: The range Doppler map  $\mathbf{G}_i$  give rise to the micro-Doppler spectrum.

The next subsection will explain how the bounds are determined.

### 2.4.1 Tracking & range gate

To produce a good micro-Doppler signature it is important that the bounds  $b_{L,i}$  and  $b_{H,i}$  are accurate. The bounds are calculated in the *Tracking & range gate* step and as the name implies tracking is a vital step in setting good bounds. Tracking a target with radar is a big subject and not really the focus of this thesis. Therefore a very simple tracking algorithm was developed and used. It got the job done in most circumstances. Table 2.4 contains the pseudocode detailing how the tracking works. As seen there it starts to check if the  $\mathbf{A}_{2,i}$  contains the largest point scatterer (in amplitude) up till that point in time. If so the position of the target is automatically set to be at the same position as that point scatterer. If not it finds the largest point scatterer that lies in a box surrounding the previous position of the target. That box is defined in range by  $N_{\text{lim}}$  and in Doppler frequency by  $\Omega_{\text{lim}}$ . Table 2.5 has the pseudocode describing how  $b_{L,i}$  and  $b_{H,i}$  are calculated. The principle behind this range gate is simple. The gate has a predefined fixed length defined as two times the half gate length denoted  $N_{\text{W}}$ . This means that  $b_{H,i} = b_{L,i} + 2 \times N_{\text{W}}$  unless the gate happens to go over one of the edges. The for-loop goes through every combination that keeps the target inside the range gate. In the end the combination that has the largest Frobenius norm  $\|\cdot\|_F$  (sum of the squared absolute value of all elements in matrix) denoted  $F$  is chosen as the range gate. In practice  $N_{\text{W}} = 13$  which means that it is assumed that the target spans about 1 meter in range.

Table 2.4: Tracking

---



---

**input**

$$\mathbf{W}_{2,i} = \begin{bmatrix} \hat{\Omega}_{0,0} & \hat{\Omega}_{0,1} & \cdots & \hat{\Omega}_{0,K-1} \\ \hat{\Omega}_{1,0} & \hat{\Omega}_{1,1} & \cdots & \hat{\Omega}_{1,K-1} \\ \vdots & \vdots & \ddots & \vdots \\ \hat{\Omega}_{N-1,0} & \hat{\Omega}_{N-1,1} & \cdots & \hat{\Omega}_{N-1,K-1} \end{bmatrix} = \{\hat{\Omega}_{n,k}\}_{k=0}^{K-1}, \quad n = 0, 1, \dots, N-1$$

and

$$\mathbf{A}_{2,i} = \begin{bmatrix} \hat{\alpha}_{0,0} & \hat{\alpha}_{0,1} & \cdots & \hat{\alpha}_{0,K-1} \\ \hat{\alpha}_{1,0} & \hat{\alpha}_{1,1} & \cdots & \hat{\alpha}_{1,K-1} \\ \vdots & \vdots & \ddots & \vdots \\ \hat{\alpha}_{N-1,0} & \hat{\alpha}_{N-1,1} & \cdots & \hat{\alpha}_{N-1,K-1} \end{bmatrix} = \{\hat{\alpha}_{n,k}\}_{k=0}^{K-1}, \quad n = 0, 1, \dots, N-1$$

**initialize**

$\tilde{\alpha}$  = recall the amplitude of the biggest point scatterer from memory

$\{n_p, \Omega_p\}$  = recall last position from memory

$\{\tilde{n}, \tilde{k}\} = \arg \max_{n,k} \{|\mathbf{A}_{2,i}|\}$

**if**  $\alpha_{\tilde{n},\tilde{k}} > \tilde{\alpha}$

$\tilde{\alpha} = \alpha_{\tilde{n},\tilde{k}}$

$n_t = \tilde{n}$

$\Omega_t = \hat{\Omega}_{\tilde{n},\tilde{k}}$

**else**

$N_{\min} = \max\{0, n_p - N_{\lim}\}$

$N_{\max} = \min\{N-1, n_p + N_{\lim}\}$

$\tilde{\mathbf{A}} = \{\hat{\alpha}_{n,k}\}_{k=0}^{K-1}, \quad n = N_{\min}, N_{\min} + 1, \dots, N_{\max}$

**repeat**

$\{\tilde{n}, \tilde{k}\} = \arg \max_{n,k} \{|\tilde{\mathbf{A}}_{2,i}|\}$

$\tilde{\Omega} = \hat{\Omega}_{\tilde{n},\tilde{k}}$

**if**  $\tilde{\Omega}$  is within the interval  $(\Omega_p - \Omega_{\lim}, \Omega_p + \Omega_{\lim})$

$\Omega_t = \tilde{\Omega}$

$n_t = \tilde{n}$

**else**

$\alpha_{\tilde{n},\tilde{k}} = 0$

**end if**

**until**  $\Omega_t$  and  $n_t$  are found

**end if**

**save to memory**  $\Omega_p = \Omega_t, n_p = n_t$  and  $\tilde{\alpha}$

**output**

$\{\Omega_t, n_t\}$

---



---

Table 2.5: Range gate

---



---

**input**

$$\mathbf{W}_{2,i} = \begin{bmatrix} \hat{\Omega}_{0,0} & \hat{\Omega}_{0,1} & \cdots & \hat{\Omega}_{0,K-1} \\ \hat{\Omega}_{1,0} & \hat{\Omega}_{1,1} & \cdots & \hat{\Omega}_{1,K-1} \\ \vdots & \vdots & \ddots & \vdots \\ \hat{\Omega}_{N-1,0} & \hat{\Omega}_{N-1,1} & \cdots & \hat{\Omega}_{N-1,K-1} \end{bmatrix} = \{\hat{\Omega}_{n,k}\}_{k=0}^{K-1}, \quad n = 0, 1, \dots, N-1$$

and

$$\mathbf{A}_{2,i} = \begin{bmatrix} \hat{\alpha}_{0,0} & \hat{\alpha}_{0,1} & \cdots & \hat{\alpha}_{0,K-1} \\ \hat{\alpha}_{1,0} & \hat{\alpha}_{1,1} & \cdots & \hat{\alpha}_{1,K-1} \\ \vdots & \vdots & \ddots & \vdots \\ \hat{\alpha}_{N-1,0} & \hat{\alpha}_{N-1,1} & \cdots & \hat{\alpha}_{N-1,K-1} \end{bmatrix} = \{\hat{\alpha}_{n,k}\}_{k=0}^{K-1}, \quad n = 0, 1, \dots, N-1$$

and

$\{\Omega_{t,n_t}\}$

**initialize**

$E = 0$

$N_{\min} = \max\{0, n_t - N_w\}$

**for**  $\tilde{n} = N_{\min}, N_{\min} + 1, \dots, n_t - 1$

$N_{\max} = \min\{N - 1, \tilde{n} + (2 \times N_w)\}$

$\tilde{\mathbf{A}} = \{\hat{\alpha}_{n,k}\}_{k=0}^{K-1}, \quad n = \tilde{n}, \tilde{n} + 1, \dots, N_{\max}$

$\tilde{F} = \|\tilde{\mathbf{A}}\|_F$

**if**  $\tilde{F} > F$

$b_{L,i} = \tilde{n}$

$b_{H,i} = N_{\max}$

$F = \tilde{F}$

**end if**

**end for**

**output**

$\{b_{L,i}, b_{H,i}\}$

---



---

### 2.4.2 Synthesize $\mu$ -Doppler signature

The STFT based micro-Doppler signature  $\mu_i$  is the sum of the gated range-Doppler map. Mathematically it is defined as

$$\mu_i = \begin{bmatrix} u_{0,0} & u_{0,1} & \cdots & u_{0,i} \\ u_{1,0} & u_{1,1} & \cdots & u_{1,i} \\ \vdots & \vdots & \ddots & \vdots \\ u_{D-1,0} & u_{D-1,1} & \cdots & u_{D-1,i} \end{bmatrix} \quad (2.51)$$

where

$$u_{d,i} = \sum_{n=b_{L,i}}^{b_{H,i}} g_{n,d} \quad (2.52)$$

As defined in table 2.2  $g_{n,d}$  denotes the entries in the range-Doppler map  $\mathbf{G}_i$ .

In addition to the STFT based micro-Doppler signature a experimental micro-Doppler signature is created with the aim of creating a signature that has improved time-frequency resolution compared to the STFT based signature. This micro-Doppler signature is based on the parameters  $\{\mathbf{W}_{1,i}, \mathbf{A}_{1,i}\}$  (the same parameters used to remove the clutter from the STFT based signature) from the RELAX algorithm and is denoted  $\xi_i$ . Table 2.6 contains the pseudocode that details how it is made. It is simply a matrix where the estimated point scatterers from  $\{\mathbf{W}_{1,i}, \mathbf{A}_{1,i}\}$  is placed in the correct corresponding Doppler frequency bin with its estimated amplitude. If the estimated point scatterer has a estimated angular normalized frequency whose absolute value  $|\hat{\Omega}_{n,k}|$  is less than a threshold  $\epsilon_f$  (which is defined to be clutter) it is left out. Finally when a section of this experimental signature is used the signature is smoothed a bit using the *imfilter* function in Matlab (not in the pseudocode).

Table 2.6: RELAX based micro-Doppler signature

---



---

**input**

$$\mathbf{W}_{1,i} = \begin{bmatrix} \hat{\Omega}_{0,0} & \hat{\Omega}_{0,1} & \cdots & \hat{\Omega}_{0,K-1} \\ \hat{\Omega}_{1,0} & \hat{\Omega}_{1,1} & \cdots & \hat{\Omega}_{1,K-1} \\ \vdots & \vdots & \ddots & \vdots \\ \hat{\Omega}_{N-1,0} & \hat{\Omega}_{N-1,1} & \cdots & \hat{\Omega}_{N-1,K-1} \end{bmatrix} = \{\hat{\Omega}_{n,k}\}_{k=0}^{K-1}, \quad n = 0, 1, \dots, N-1$$

and

$$\mathbf{A}_{1,i} = \begin{bmatrix} \hat{\alpha}_{0,0} & \hat{\alpha}_{0,1} & \cdots & \hat{\alpha}_{0,K-1} \\ \hat{\alpha}_{1,0} & \hat{\alpha}_{1,1} & \cdots & \hat{\alpha}_{1,K-1} \\ \vdots & \vdots & \ddots & \vdots \\ \hat{\alpha}_{N-1,0} & \hat{\alpha}_{N-1,1} & \cdots & \hat{\alpha}_{N-1,K-1} \end{bmatrix} = \{\hat{\alpha}_{n,k}\}_{k=0}^{K-1}, \quad n = 0, 1, \dots, N-1$$

and

$\{b_{L,i}, b_{H,i}\}$

**initialize**

$z_i[d] = 0, \quad d = 0, 1, \dots, D-1$

**for**  $n = b_{L,i}, b_{L,i} + 1, \dots, b_{H,i}$

**for**  $k = 0, 1, \dots, K-1$

**if**  $|\hat{\Omega}_{n,k}| < \epsilon_f$

$\tilde{f}_d = \frac{\hat{\Omega}_{n,k} f_p}{2\pi}$

$\tilde{d} = \text{round}\{\tilde{f}_d \times \frac{D}{f_p}\}$

$z_t[\tilde{d}] = |\hat{\alpha}_{n,k}|$

**end if**

**end for**

**end for**

**output**

$$\xi_i = \begin{bmatrix} z_0[0] & z_1[0] & \cdots & z_i[0] \\ z_0[1] & z_1[1] & \cdots & z_i[1] \\ \vdots & \vdots & \ddots & \vdots \\ z_0[D-1] & z_1[D-1] & \cdots & z_i[D-1] \end{bmatrix}$$


---



---

Both the STFT and RELAX based micro-Doppler signatures are subject to quite heavy fluctuation in the targets intensity (mainly dependent on range). To counter this every time bin (column) of the signatures are normalized to have almost the same maximum amplitude.

## 2.5 Gait-Doppler Map (feature extraction)

The term gait (not to be confused with gate) is a term applies to the pattern of movements of the limbs of animals and humans. Most of the time it can be thought of as “walking pattern”. The pattern which a animal uses to walks can vary from specie to specie common to all of them is that they repeat to bring the animal forward. One cycle before the pattern starts over again is referred to as a gait cycle. The gait-Doppler map is used to estimate the frequency of the gait cycle called the fundamental gait frequency denoted  $f_g$ .

The gait-Doppler map is simply created by taking the FFT of the rows of the micro-Doppler signatures. This means that the gait-Doppler map share the column dimension with the range-Doppler signature which is the Doppler frequency spectrum. The gait-Doppler map can also be used to find the average velocity/Doppler shift of the target.

## Results & discussion

### 3.1 Test setup

The system was tested in a big garden depicted in figure 3.1. The radar is situated in the middle of the *red* circle. The radars direction line is marked with the *blue* line and is simply the direction the radar is pointing meaning it is the direction the main beam of the radar is pointed. Finally the inner and outer limit of the frame span is illustrated with the two *green* lines. Note that the dog is between the two lines and therefore inside the radars frame span (would therefore be detectable). The only clutter source of note in this setup was the ground, in addition there was very little multipath interference. Figure 3.2 shows a birds eye drawing of the same test setup. Just as the picture above the radar is in the middle of a red circle, the radar direction line is blue and the green lines are the limits of the frame span. In addition the target path (the route the target used during the test) is illustrated with a black line. The targets (including the dog) paths was made to *always* cross the direction line at roughly the same point called the common intersection point (small black cir-

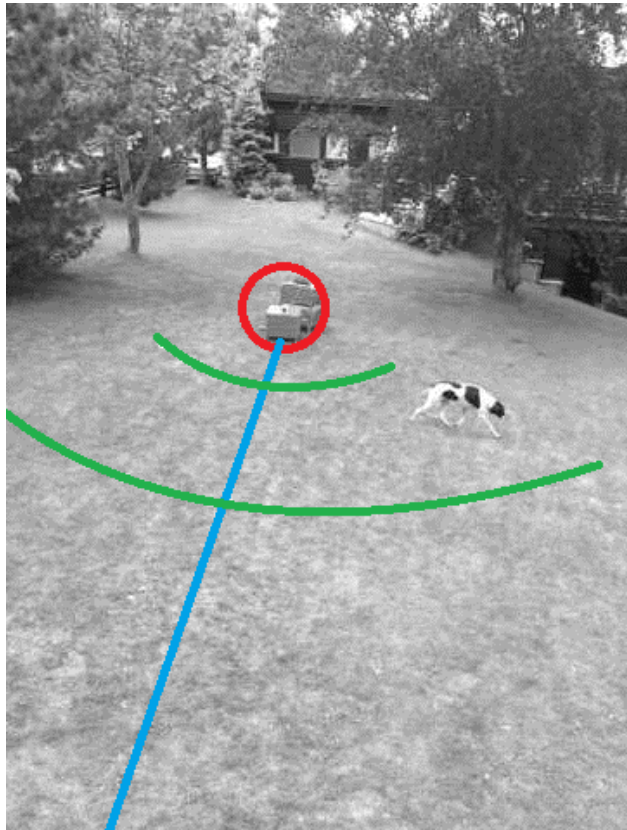


Figure 3.1: Annotated picture of the test setup. Radar circled in red. Radar direction line in blue. Frame span inner and outer limit in green

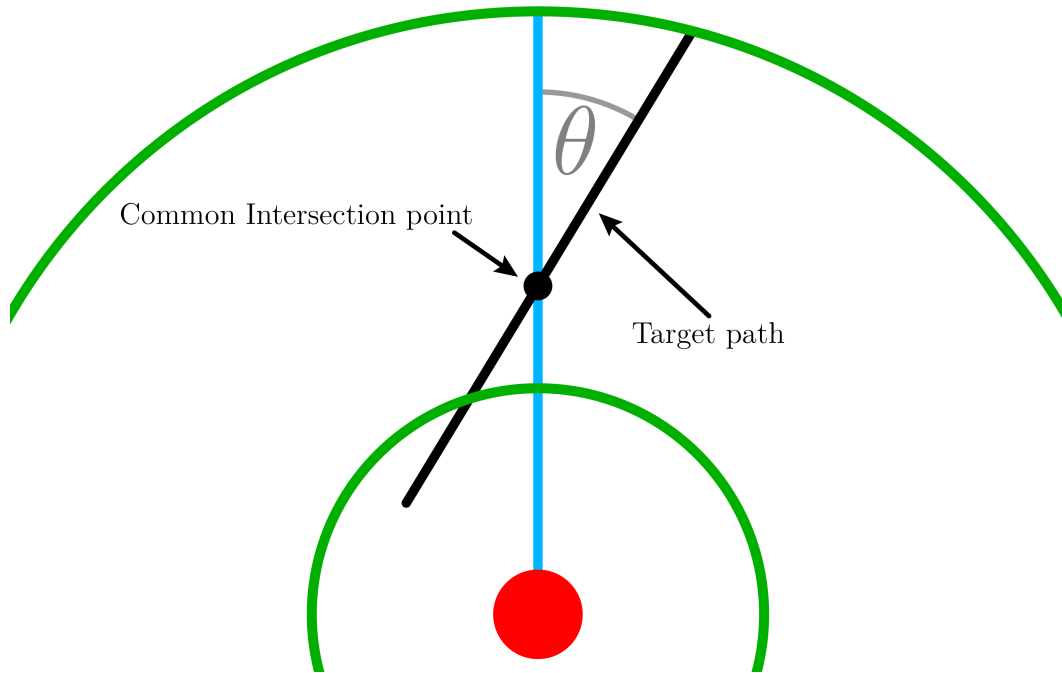


Figure 3.2: Birds eye illustration of the test setup, showing the common intersection point and the target path angle  $\theta$

cle). This point was chosen to not be in the middle of the frame span but a bit closer to the radar. This means that a targets specific route can be defined by a single angle the target path angle  $\theta$ . It is defined as the angle (grey in the figure) between the radar direction line and the target path. For example is the target path angle is  $\theta = 0$  the target would be moving along the radar direction line.

## 3.2 Micro-Doppler signatures

The first and most important results that will be discussed is the micro-Doppler signatures. First the challenges identified with producing the micro-Doppler signature will be discussed. Then the human micro-Doppler signature and the effects of different window sizes will be discussed. After that micro-Doppler signatures from the dog will be presented and discussed.

### 3.2.1 Human Signature & the Effects of Window Length

On the following pages the same human micro-Doppler signature is depicted over and over again from figure 3.3 to 3.7 (nor 3.8) with changing window length ( $M_1 \times T$ ). Both the STFT based micro-Doppler and the more experimental RELAX based micro-Doppler signature is shown for each window length. In these signatures a adult woman is moving inbound along the direction line ( $\theta = 0^\circ$ ). The most striking pattern that is seen in all figures is the “zig-zag” pattern from the high intensity (dark red) areas.

This pattern is created by the reflections from the torso and shows that the torso of person does not have a constant speed during walking. The limbs create weaker “spikes” protruding from the torso zig-zag. This is expected since the limbs alternate between moving slower and moving faster than the torso when walking. The highest and strongest spikes probably corresponds to the legs that normally moves faster than the arms (mainly because they are longer) and since they have a larger Radar Cross Section (RCS) compared to the arms. Observe that the spikes (legs) tend to come out as the torso is in a local valley in its Doppler frequency (speed). This means that the torso is moving at its slowest when the foot moving forward is at its fastest. Correspondingly the torso is moving at its fastest as the forward moving foot has stopped or almost stopped and the weight of the body is being shifted to it.

As all the figures show the window length has a big effect on the micro-Doppler signature. Figure 3.3 is produced with the smallest window used in this thesis lasting just 5 pulses equivalent to about 71.4 ms. There a lot of leakage in the STFT Doppler spectrum and the aliasing is apparent. This signature has the greatest sensitivity for frequency change provided by its excellent time resolution. The RELAX based signature has as expected better frequency resolution and is perhaps a little bit easier for a human to identify structures and patterns. However it still struggles with quite some spread in the “dots” it has estimated. If this spread represent the underlining structure of the signal and is just not estimator noise there seems to be no easy way to make immediate sense of the structure. Note the band around 0 Hz in the RELAX based signature that shows the band where the clutter has been removed. This band has been removed in its STFT counterpart as outlined previously but the leakage of the Doppler spectrum masks this making it seem like no clutter has been removed. As the window length gets longer the removed clutter band in the STFT becomes more apparent. The increasing window length provide better and better frequency resolution and the more fine structure in the Doppler frequency dimension emerges. The time resolution suffers however although it may be less apparent. Figure 3.7b showing the RELAX based signature with a window of 0.4 seconds may look impressive with a lot of details of different scatterers but a lot of it is probably heavily corrupted by the relative large time scale. Still it seems that with a slowly walking person the window length can safely be used up to 0.2 seconds and perhaps more depending on the use.

Figure 3.8 shows the signature of a man slowly walking outbound with a target path angle of about  $60^\circ$ . The signature is similar in nature to the one discussed earlier but here the target seem to accelerate between the first and third second judging by the rising torso zig-zag. In this case the acceleration does not come from the target moving faster but is a result of the targets path. The first second the target is moving close to the radar and with a  $\theta = 60^\circ$  the radial velocity of the target seen from the radar is small. As the target moves away from the radar the Line Of Sight (LOS) between the radar and the target becomes more and more aligned with the target path

and more of the targets movement is in the direction of the radar. This result in larger radial velocity and higher Doppler frequencies. This goes for the limbs as well that has smaller spikes in the beginning of the signature compared to the end. This “aligning” effect dies out around the 3 seconds mark as the angle between the LOS and target path changes less and less. If the target was moving Inbound instead the effect would be the same except in reverse and the target would seem to slow down.

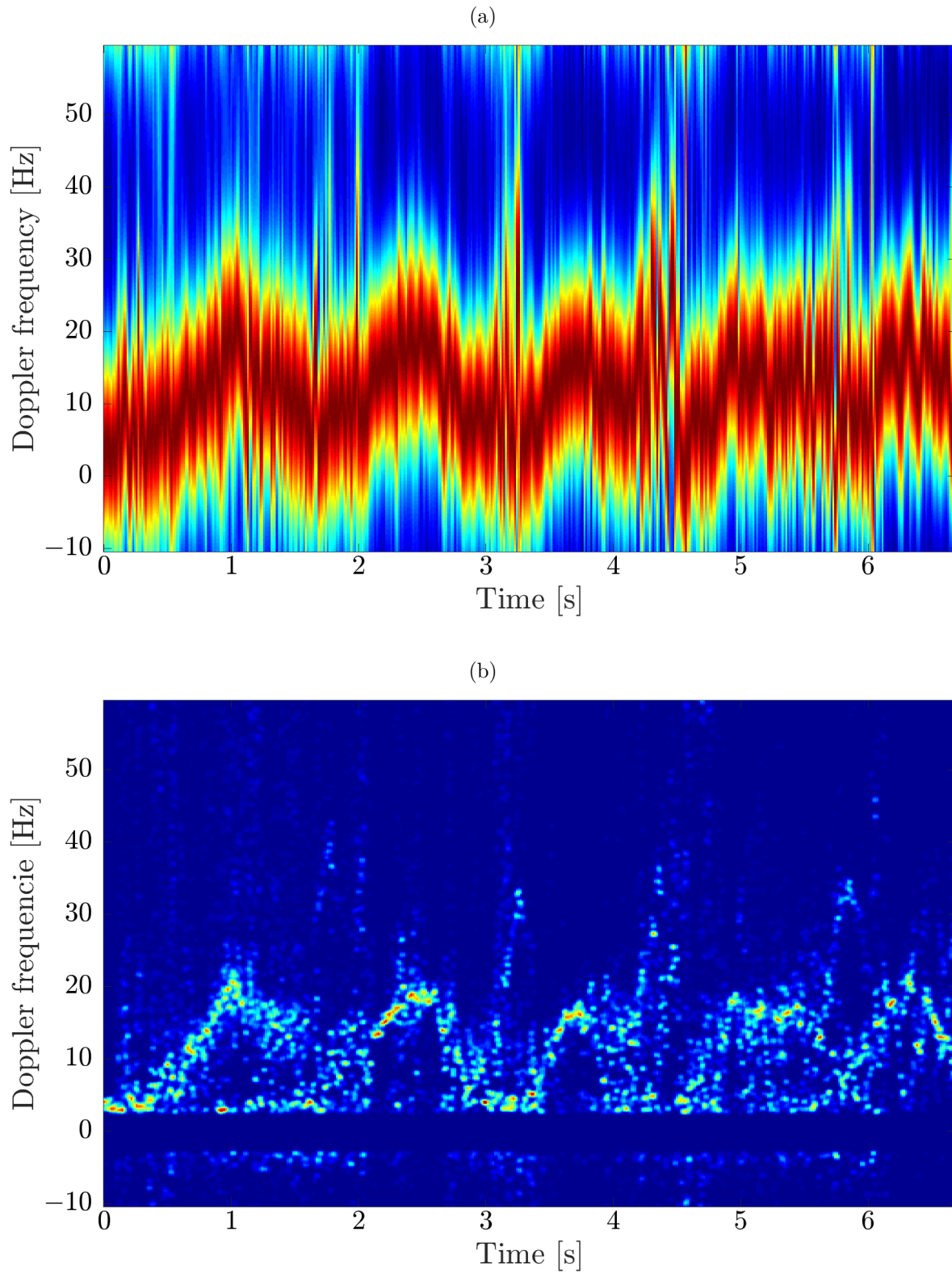


Figure 3.3: Micro-Doppler signature based on FFT (a) & RELAX (b) of a woman slowly walking with an inbound direction.  $\theta = 0^\circ$ . Window length 71.4 ms

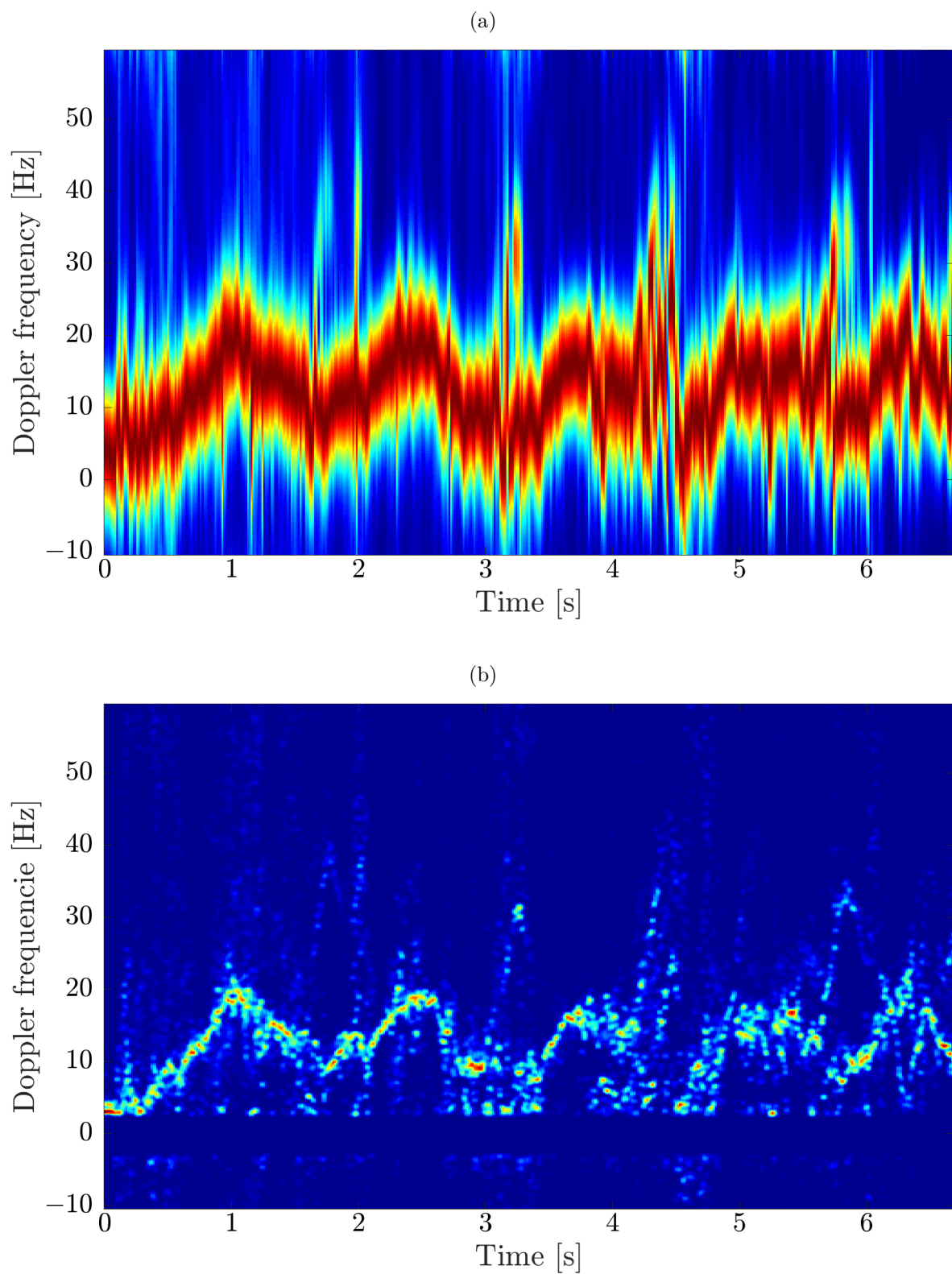


Figure 3.4: Micro-Doppler signature based on FFT (a) & RELAX (b) of a woman slowly walking with an inbound direction.  $\theta = 0^\circ$ . Window length 0.1 seconds

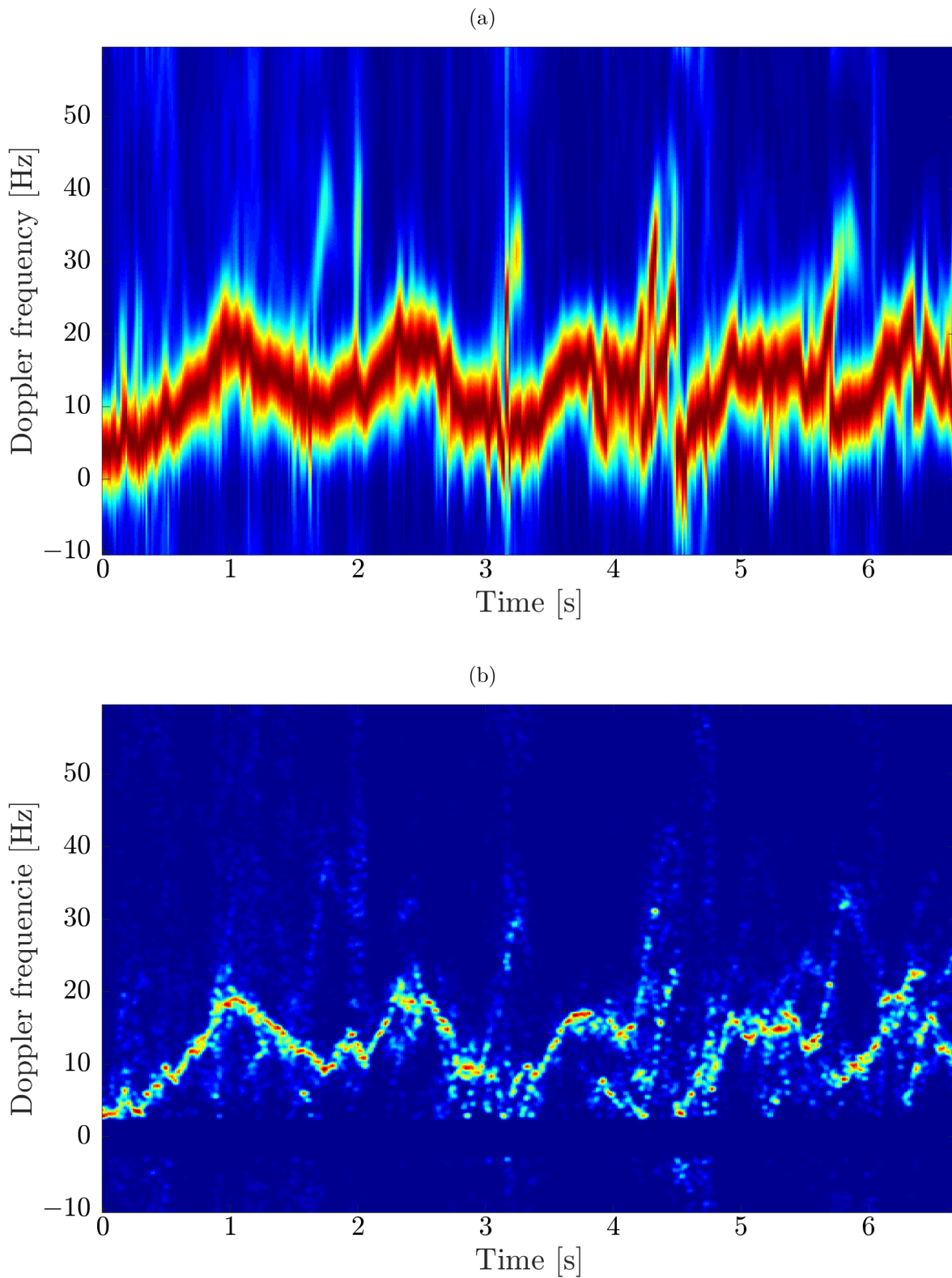


Figure 3.5: Micro-Doppler signature based on FFT (a) & RELAX (b) of a woman slowly walking with an inbound direction.  $\theta = 0^\circ$ . Window length 0.143 seconds

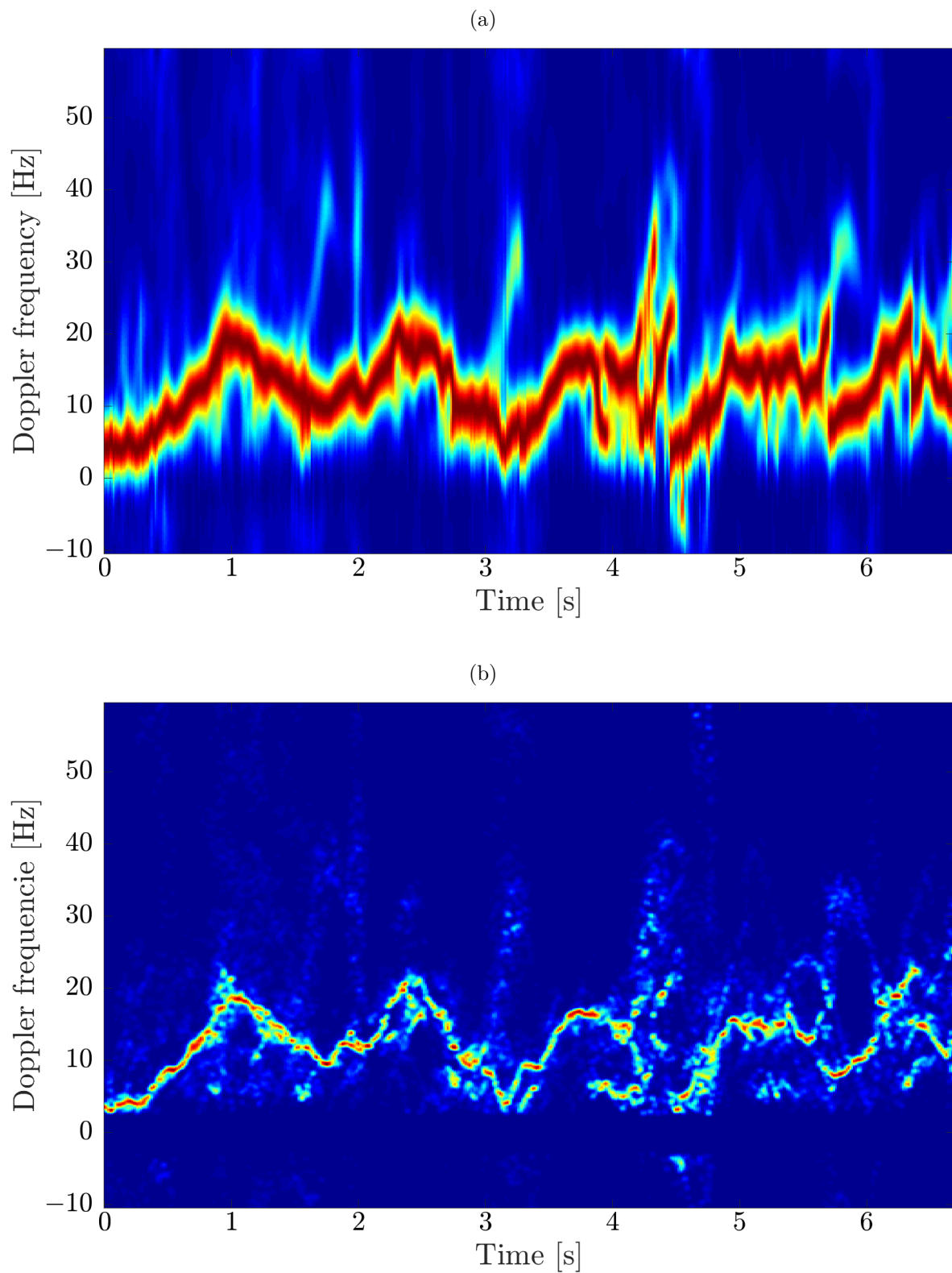


Figure 3.6: Micro-Doppler signature based on FFT (a) & RELAX (b) of a woman slowly walking with an inbound direction.  $\theta = 0^\circ$ . Window length 0.2 seconds

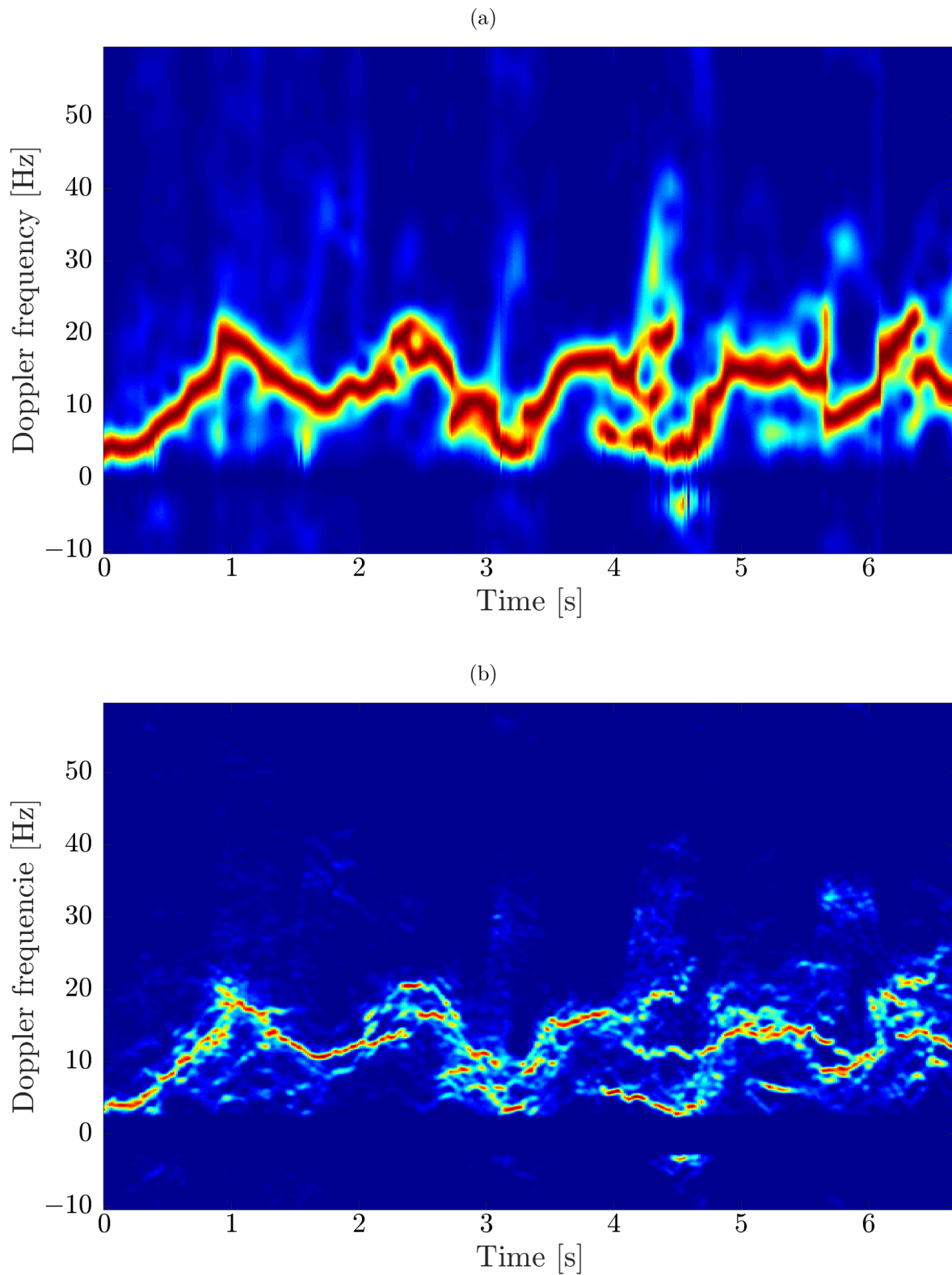


Figure 3.7: Micro-Doppler signature based on FFT (a) & RELAX (b) of a woman slowly walking with an inbound direction.  $\theta = 0^\circ$ . Window length 0.4 seconds

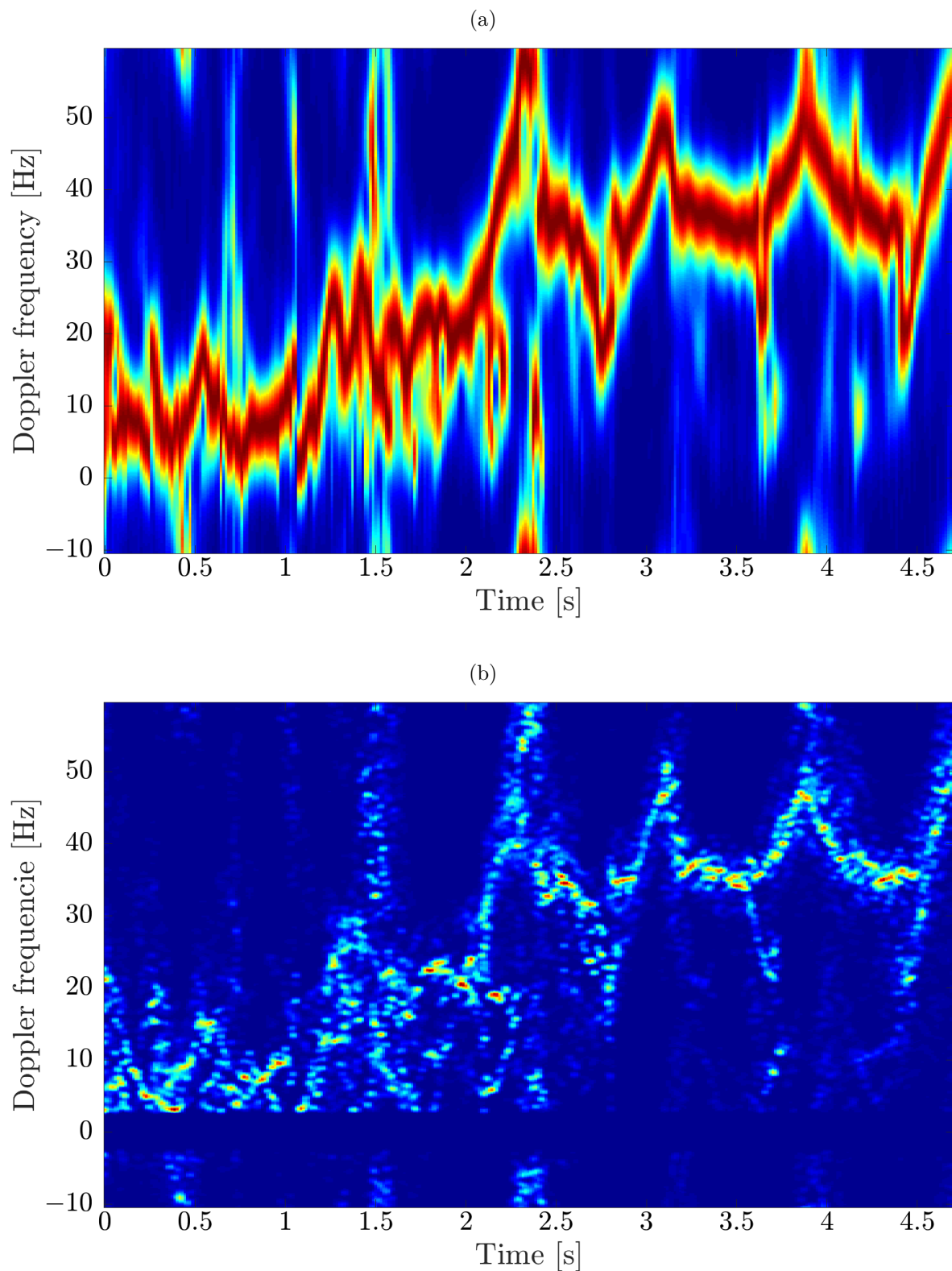


Figure 3.8: Micro-Doppler signature based on FFT (a) & RELAX (b) of a man slowly walking with a outbound direction.  $\theta = 60^\circ$ . Window length 0.143 seconds

### 3.2.2 Dog signature

The dog used for testing is depicted in figure 3.9. It is a medium sized dog of the pointer breed. From the nose to the tail the dog is about 110cm (90cm without the tail).



Figure 3.9: Picture of the dog used for the tests, a medium sized pointer.

The figures 3.10 to 3.13 focus on the same micro-Doppler signature created with different window lengths (only up to 0.2 seconds this time). Again both the STFT based and RELAX based signatures are displayed. The signatures from the dog was more sensitive to aliasing simply because the getting the dog to move slow enough was a challenge. However in the first signature presented in the dog mostly moves slow enough to not create a lot of aliasing. In fact at about the 0.8 seconds mark the dog stands mostly still and most of its echoes are removed by the clutter removal. Since the micro-Doppler signature is normalized to have almost the same maximum amplitude at each *time* bin the noise is amplified when the dogs echos are removed and a noticeable vertical line is produced that could be mistaken for a fast moving limb but is in fact mostly noise. The dog micro-Doppler signature looks a lot like the human one with a torso that creates a high intensity zig-zag line across the signature and the limbs creating spikes. The limb pattern is however a bit shorter and narrower in time (sharper spikes) compared to the human limb pattern. This is because the dogs limbs are shorter and accelerates and decelerate quicker than their human counterparts.

The figure 3.14 shows a more typical dog signature obtained from the test in that the dog is moving faster and with a lot more aliasing, before it slows down at the end.

The dog is walking outbound in this case with  $\theta = 0^\circ$ .

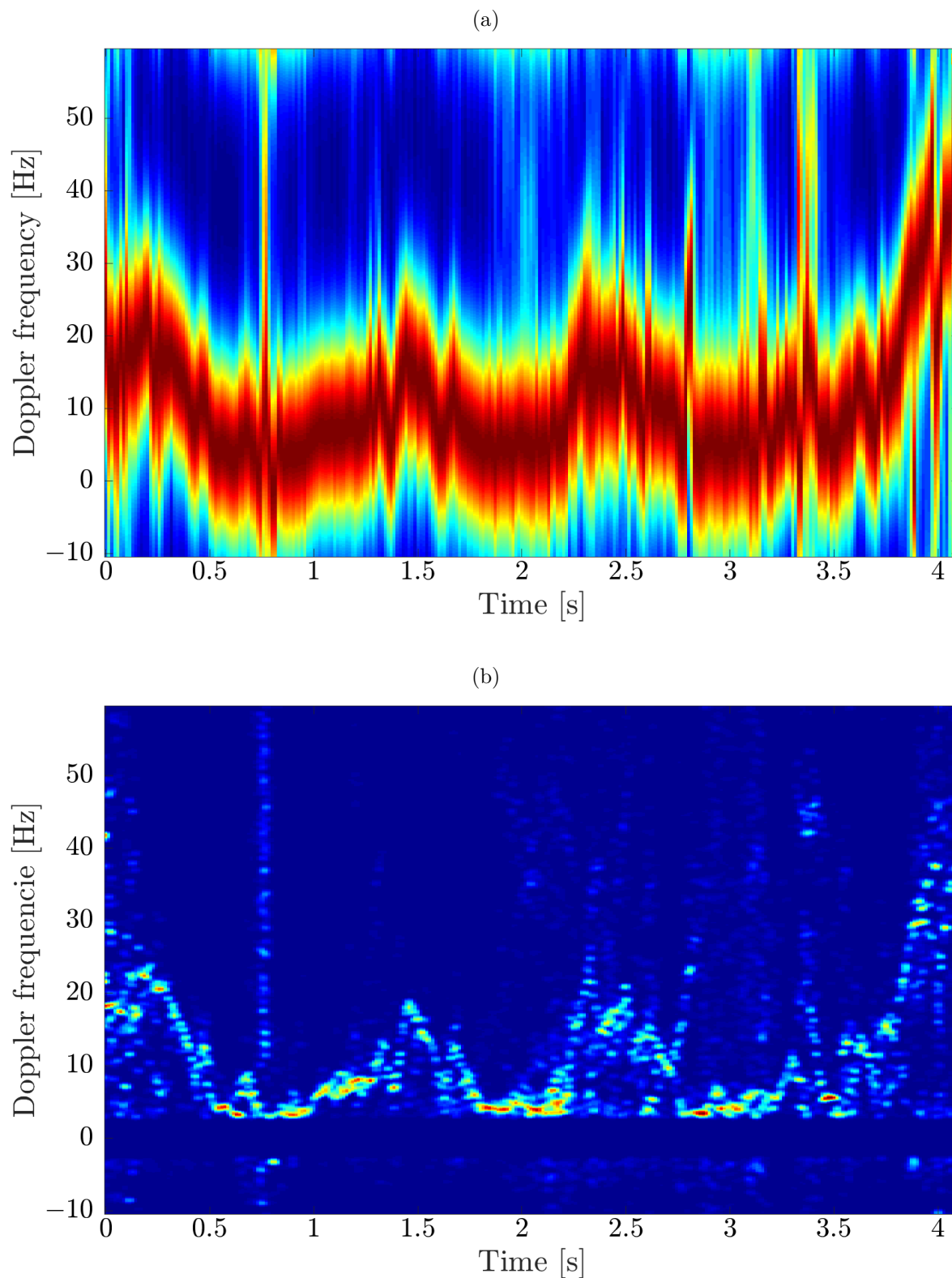


Figure 3.10: Micro-Doppler signature based on FFT (a) & RELAX (b) of a dog slowly walking with a outbound direction.  $\theta = 10^\circ$ . Window length 0.071 seconds

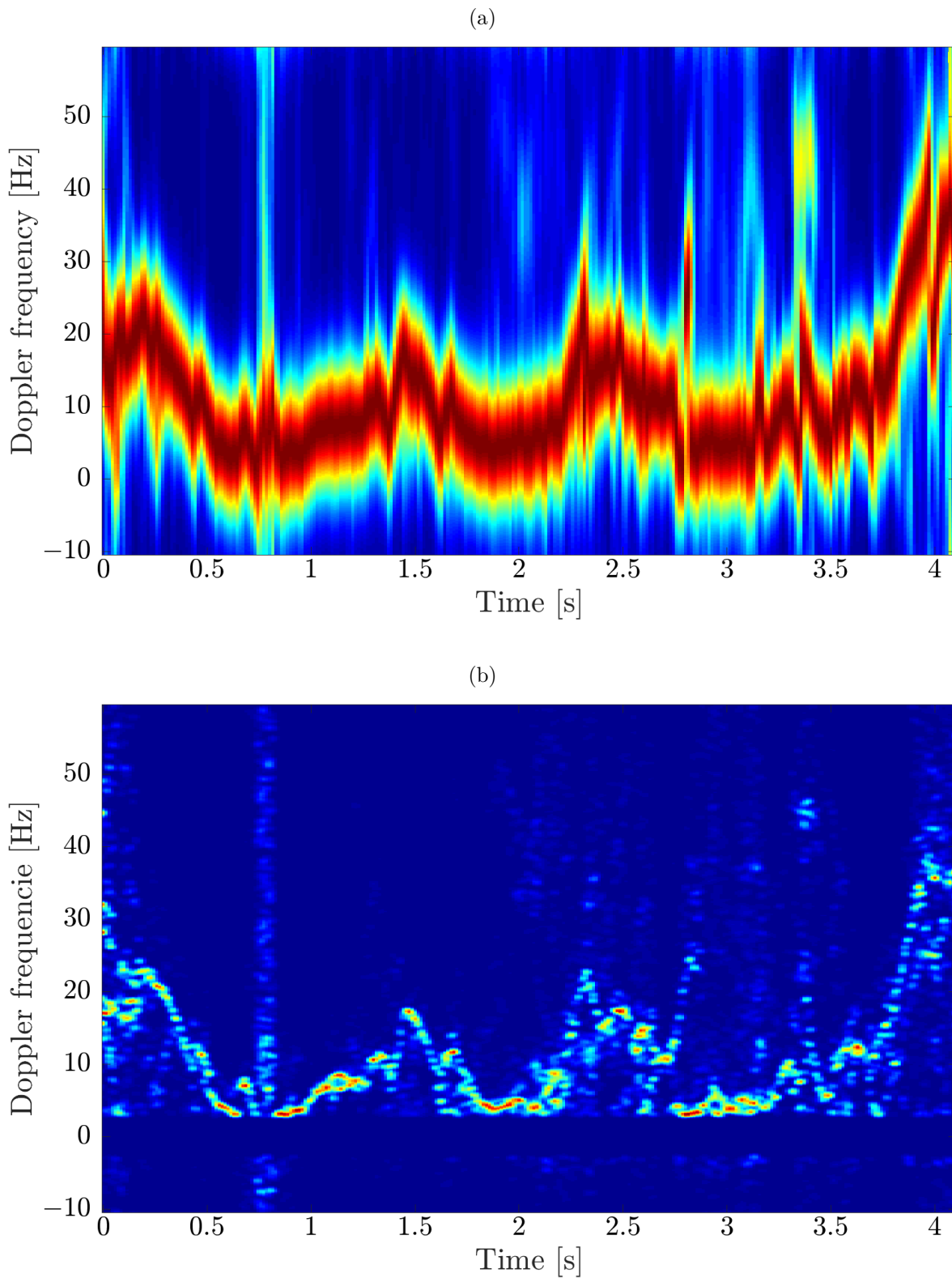


Figure 3.11: Micro-Doppler signature based on FFT (a) & RELAX (b) of a dog slowly walking with a outbound direction.  $\theta = 10^\circ$ . Window length 0.1 seconds

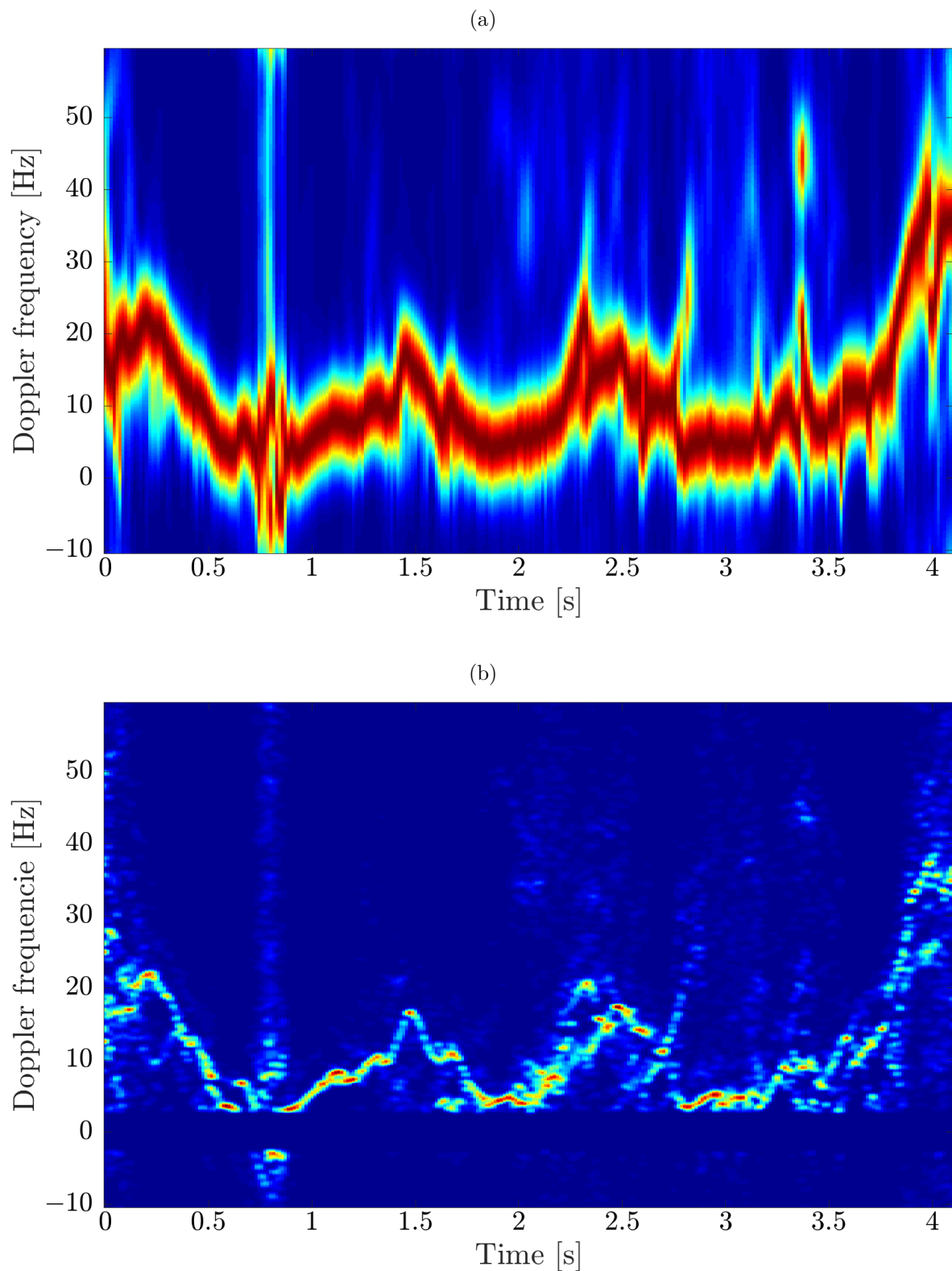


Figure 3.12: Micro-Doppler signature based on FFT (a) & RELAX (b) of a dog slowly walking with a outbound direction.  $\theta = 10^\circ$ . Window length 0.143 seconds

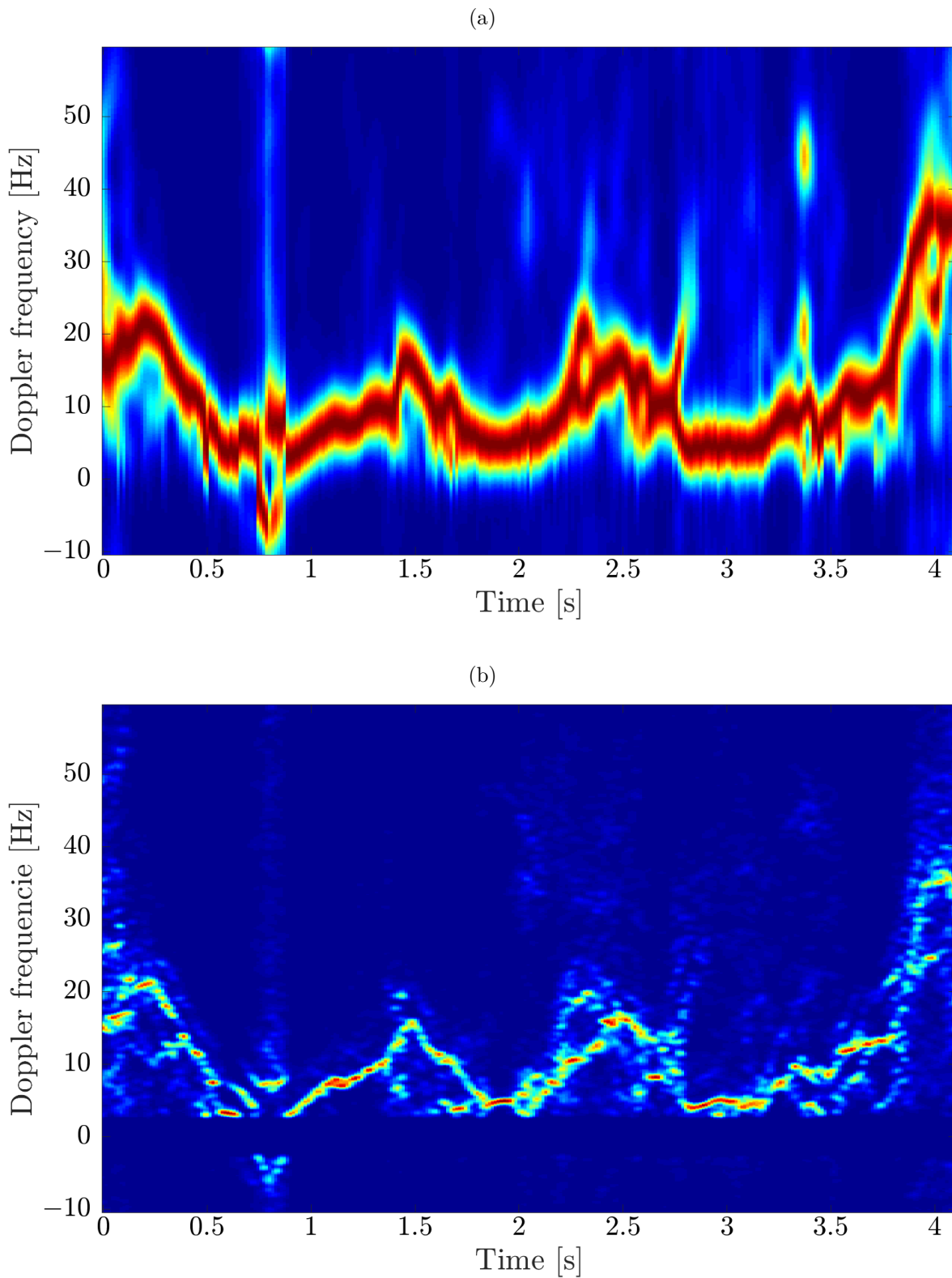


Figure 3.13: Micro-Doppler signature based on FFT (a) & RELAX (b) of a dog slowly walking with a outbound direction.  $\theta = 10^\circ$ . Window length 0.2 seconds

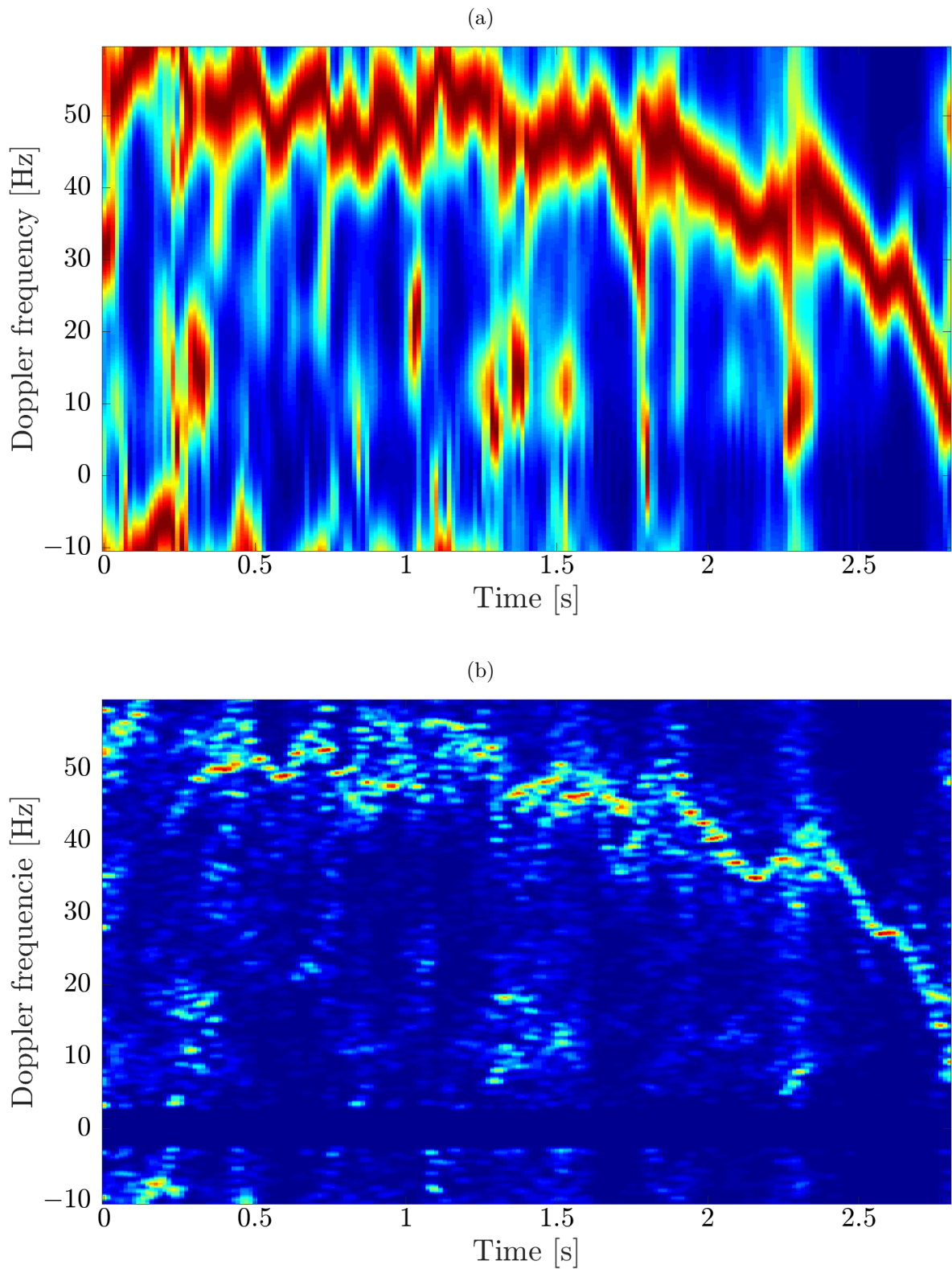


Figure 3.14: Micro-Doppler signature based on FFT (a) & RELAX (b) of a dog walking with a outbound direction.  $\theta = 0^\circ$ . Window length 0.143 seconds

### 3.3 Gait-Doppler Map & features

As mentioned in chapter 2 the gait-Doppler map is obtained by taking the row-FFT of the micro-Doppler signature.

#### 3.3.1 Gait-Doppler Map from Human

The figure 3.15a shows the same micro-Doppler signature used earlier of a woman slowly walking inbound with  $\theta = 0^\circ$  and with its corresponding gait-Doppler map which has had its DC component removed. Three features are labeled in the gait-Doppler map the ② is the fundamental gait-frequency  $f_g$ , ③ and ④ is its harmonics. Produced by the moving limbs and torso. Figure 3.15b shows the same gait-Doppler map where the DC has not been removed. This makes it possible to observe feature ① which is the average Doppler frequency of the torso  $f_{av}$ . With  $f_{av}$  and  $f_g$  we can define the stride which is the length the foot moves each step the target takes as

$$\text{stride} = L_s = \frac{v_{av}}{f_g} = \frac{f_{av}\lambda}{2f_g} \quad (3.1)$$

where  $v_{av}$  is the average velocity of the torso and  $L_s$  is the length of the stride in meters. In the case of the current signature  $f_g \approx 0.75\text{Hz}$  and  $f_{av} \approx 12.5\text{Hz}$  yielding a  $L_s \approx 0.36\text{meter}$ . Since the length of the limbs of human and animal are different it should be possible to separate humans and dogs by knowing their stride. The shorter legs of the dogs means it can't take as long steps as a human. The stride however will change depending how fast the animal is moving so all three features  $f_g$ ,  $f_{av}$  and  $L_s$  should be considered.

Figure 3.16a shows the same signature but based on RELAX and its gait-Doppler map as 3.15a. The fundamental gait frequency is still observable but its harmonics are harder to spot, it does not seem better in any particular way. Figure 3.16b contains the micro-Doppler signature and the gait-Doppler map of the man discussed earlier which was moving outbound with  $\theta = 60^\circ$ . In this case will the increasing speed due to the "aligning effect" create a low frequency component that could be mistaken for the fundamental gait frequency. The true fundamental gait frequency and its harmonics are still observable however. That the radial speed is dependent on the  $\theta$  means that all the average Doppler frequency  $f_{av}$  is such a robust feature that one would like. By extension this also applies to the stride length  $L_s$ . Observing the target over time can somewhat mitigate this challenge.

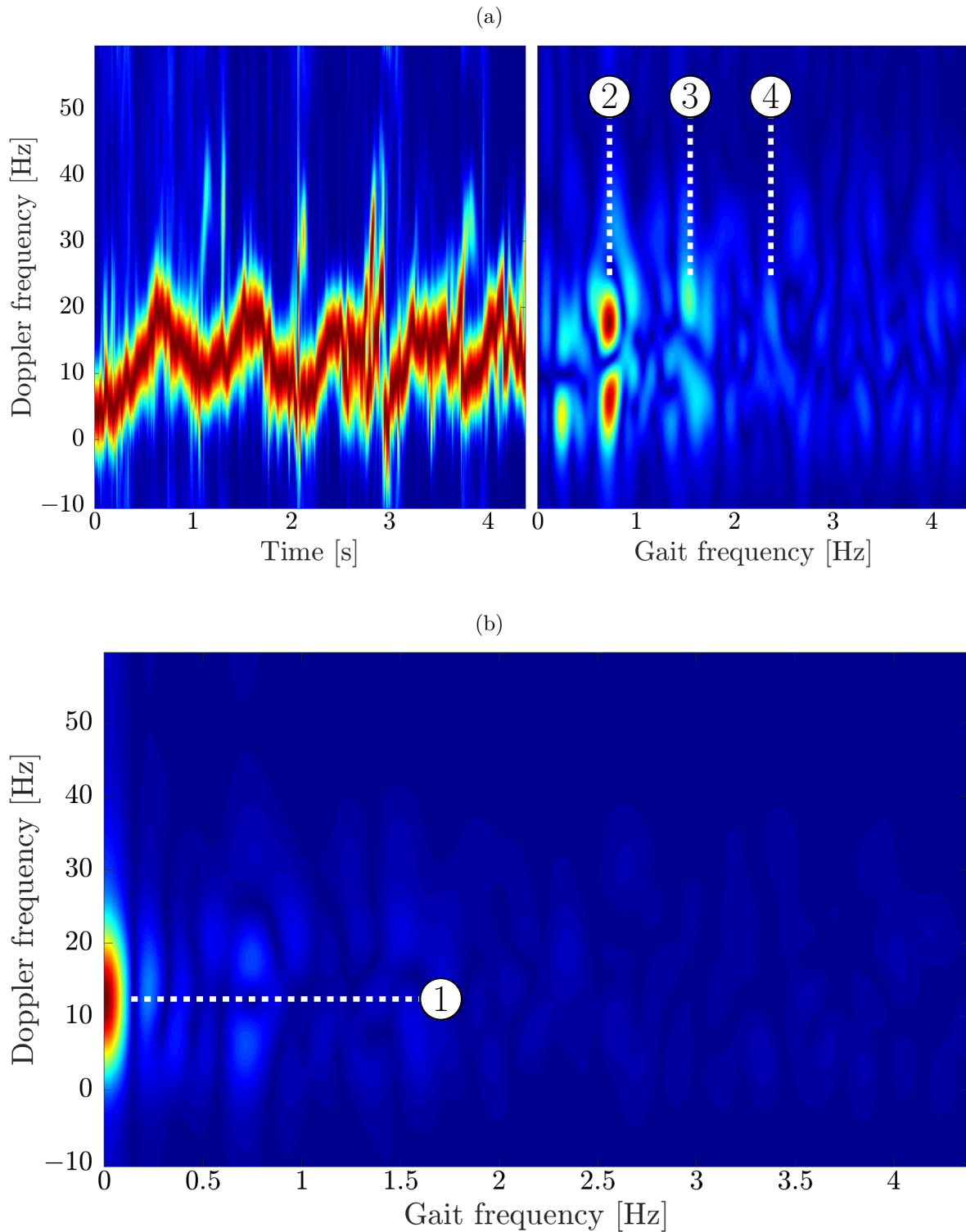


Figure 3.15: Gait-Doppler Map (DC - removed) and micro-Doppler signature of woman slowly walking with an inbound direction.  $\theta = 0^\circ$ . Window length 0.143 seconds (a) & (b) The same Gait-Doppler map but with the DC intact. Features in the gait-Doppler map has been labeled.

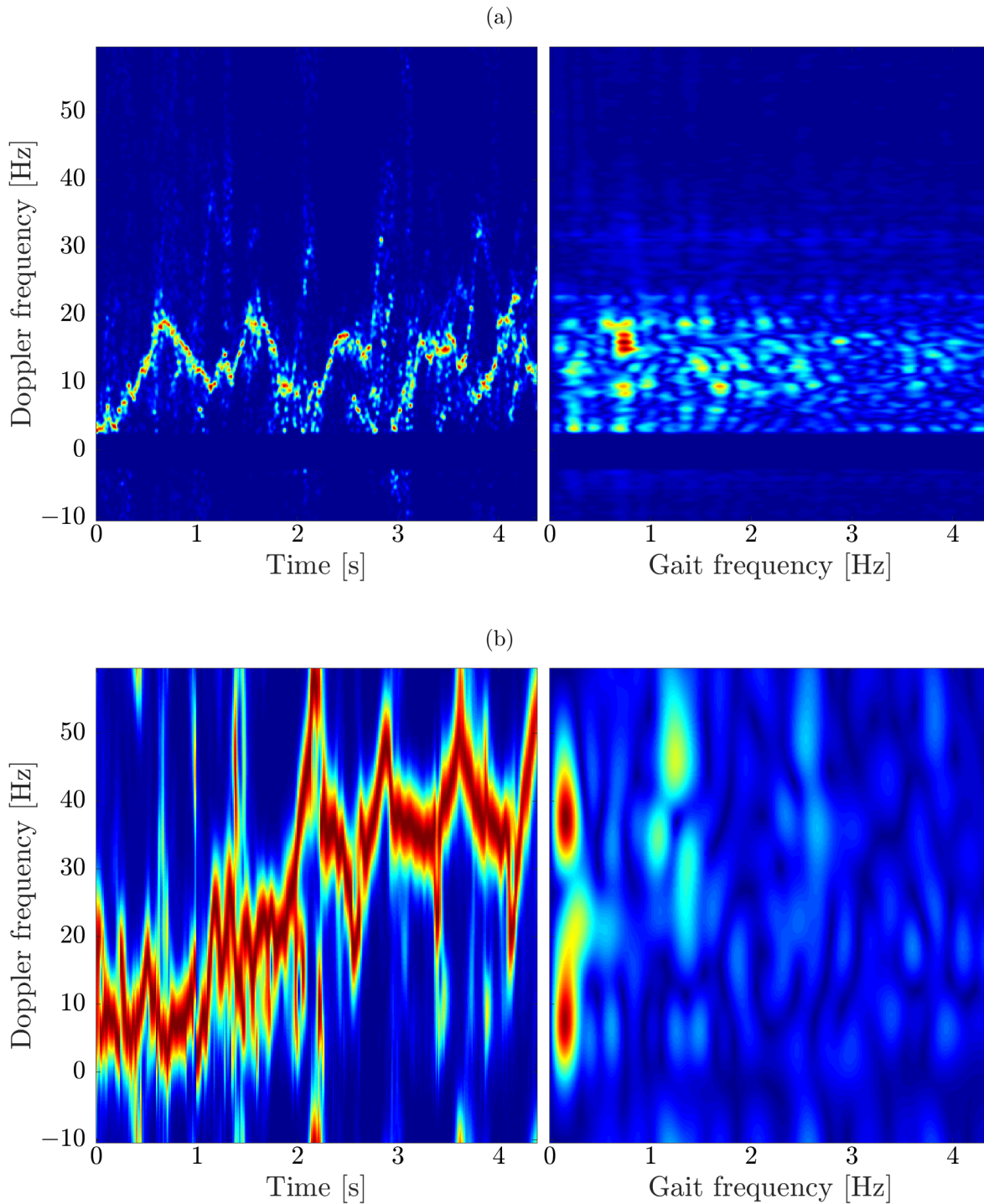


Figure 3.16: Gait-Doppler Map (DC - removed) and micro-Doppler signature of woman slowly walking with a inbound direction both based on the RELAX algorithm.  $\theta = 0^\circ$ . Window length 0.143 seconds (a) & (b) Gait-Doppler Map (DC - removed) and micro-Doppler signature of a man slowly walking with a outbound direction.  $\theta = 60^\circ$ . Window length 0.143 seconds.

### 3.3.2 Gait-Doppler Map from Dog

Figure 3.17a is the same dog micro-Doppler signature discussed earlier and its gait-Doppler map. The dog is moving slowly outbound (stopping a short while) and  $\theta = 10^\circ$ . The dogs fundamental gait  $f_g$  is easy to pick out and is approximately 0.83 Hz. It is however harder to spot its harmonics. Below figure 3.17b is the same gait-Doppler map but with the DC intact and the average Doppler frequency  $f_{av}$  of the dog is about 8 Hz. This means that the stride  $L_s$  is around 0.21 meters. Figure 3.18a shows the same signature and gait-Doppler map as figure 3.17a but based on the RELAX algorithm. This gait-Doppler map does not seem much better, the harmonics of the fundamental gait frequency is maybe a bit easier to pick out. Finally there is figure 3.18b also a signature looked at earlier with its gait-Doppler map. The dog as mentioned is here walking normally with  $\theta = 0^\circ$ . Just as seen with figure 3.16b the “radically” changing radial speed of the target create low frequency components in the gait-Doppler map that could be mistaken for the fundamental gait-frequency. Also it is not clear by looking at the gate-Doppler map what  $f_g$  really is.

Table 3.1: Feature Comparisons

	Woman	Dog
Fundamental gait frequency $f_g$	0.75 Hz	0.83 Hz
Average Doppler frequency $f_{av}$	12.5 Hz	8Hz
Stride length $L_s$	0.36 m	0.21 m

Table 3.1 compares the features obtained from the from the woman and dog gait-Doppler map. Notice that even if the dog is moving at a lower speed than the woman it has a higher fundamental gait frequency. This is reflected by the stride length which is shorter compared to the woman.

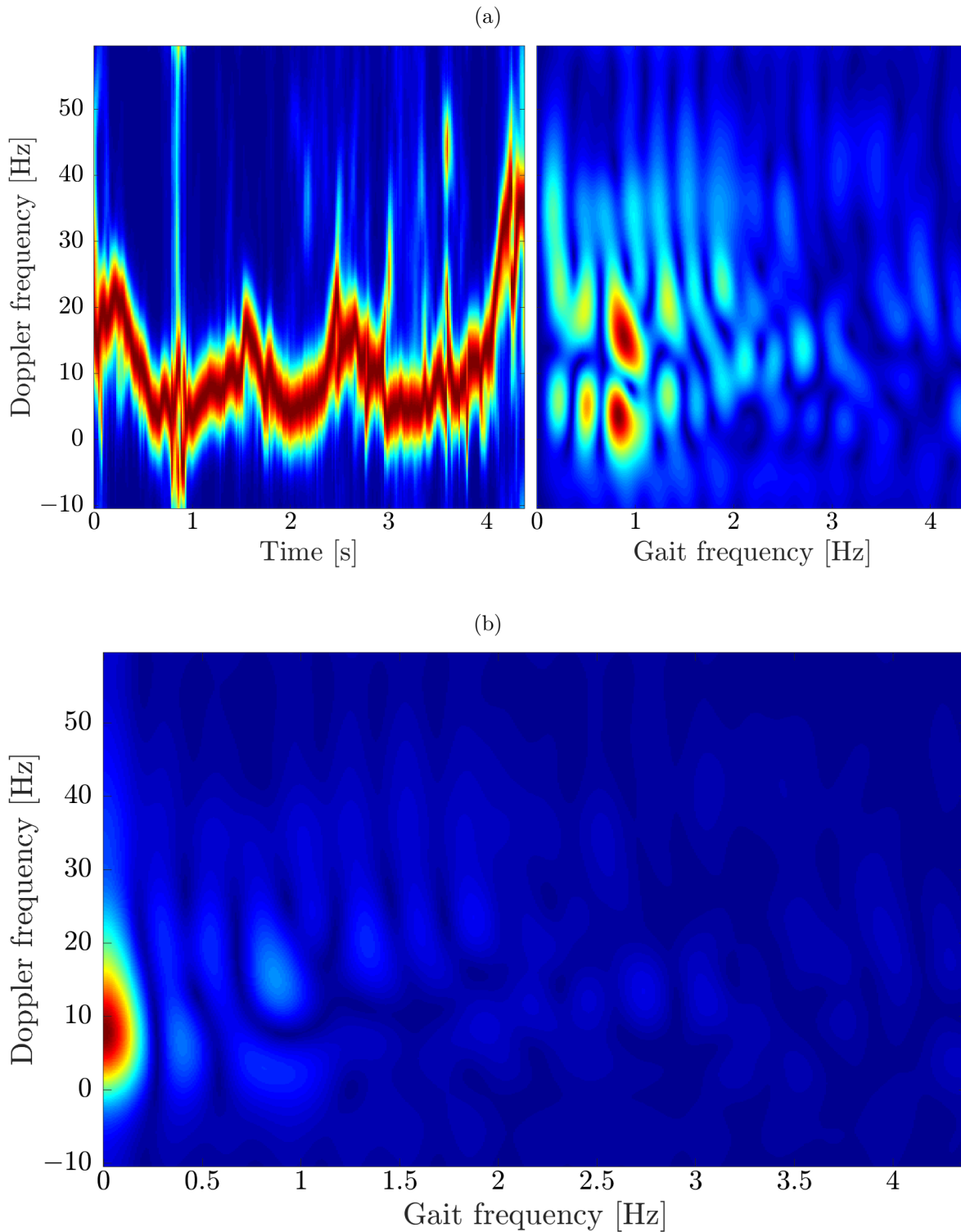


Figure 3.17: Gait-Doppler Map (DC - removed) and micro-Doppler signature of a dog slowly walking with an outbound direction.  $\theta = 10^\circ$ . Window length 0.143 seconds (a) & (b) The same Gait-Doppler map but with the DC intact.

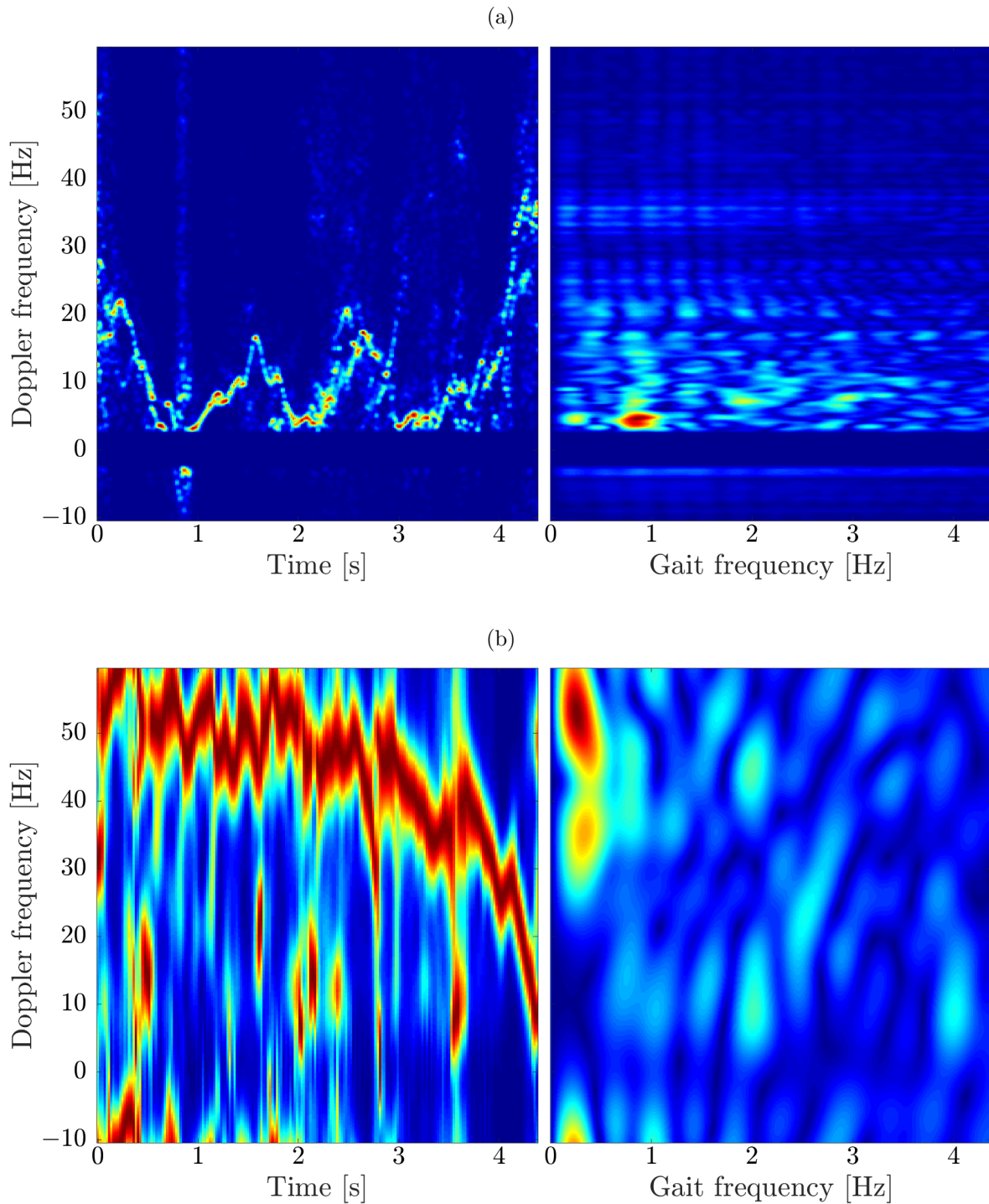


Figure 3.18: Gait-Doppler Map (DC - removed) and micro-Doppler signature of a dog slowly walking with a outbound direction both based on the RELAX algorithm.  $\theta = 10^\circ$ . Window length 0.143 seconds (a) & (b) Gait-Doppler Map (DC - removed) and micro-Doppler signature of a dog walking with a outbound direction.  $\theta = 0^\circ$ . Window length 0.143 seconds.

### 3.3.3 Challenges

The greatest problem with the micro-Doppler signature in this test was aliasing in the Doppler spectrum due to the pulse repetition frequency  $f_p$  being limited to 70 Hz. As was shown in chapter 2 the induced Doppler frequency from a target/point scatterer is dependent on its radial speed. This limit in the radar was known before hand and the plan was to make the targets move slow enough that there would be little or no aliasing. This worked okay when observing humans but getting the dog to move slow enough was a problem.

The signal to noise ratio seemed to be good enough for both adult human and the dog. The SNR was however noticeably worse for the dog and the in the test done the range was never more than 4.4 meters. At any range greater than that or if the animal is smaller than the dog used here caution regarding the SNR is advised. Other preliminary testing done indoors revealed that multipath interference could contribute to the micro-Doppler signature and should therefore be taken into account.

The tracking and range-gating worked well most of the time and is vital to achieve a good micro-Doppler signature. Tests showed that if clutter as not removed it would often dominate the signature so removing it often vital.

As discussed two of the features  $L_s$  and  $f_{av}$  is sensitive to the angle between the target path and radar LOS. This reduces their usefulness as features for classification.

## Concluding remarks

### 4.1 Further work

To create a robust system that can separate between humans and dogs let alone other animals will require further work based on the results from this thesis. Consider the overall problem, figure 1.1 can be of help here, in this thesis focus has been on the Doppler information represented by the micro-Doppler signature, but the output of the time-frequency transforms does contain data about the range as well. Using the range information in addition would mean more diversity in the collected features and the classifier would almost surely perform better. When it comes to the classifier (which was not treated in this thesis) a database of human and animal radar data should be collected so training of the classifier and testing different approaches can be performed effectively.

When it comes to the time-frequency resolution of the STFT it can be improved either by using a super-resolution algorithm like RELAX or through one of the many other time-frequency transforms like the TFDS [2] that can gradually trade better time-frequency resolution in return for more and more cross-term interference. The RELAX algorithm worked well both when used for tracking and clutter removal, however it can be quite computationally demanding. This can be remedied in several ways. Calculating the same amount of complex sinusoids every time the algorithm is used is ineffective and some way of determining how many should be estimated would probably be beneficial. The algorithm itself can also be made more effective by following this [8] paper.

The micro-Doppler signature worked well enough in this thesis but it can be improved. For example instead of a range-gate which includes everything inside it, an algorithm that only includes targets/point scatterers that is above a certain threshold in the signature could be used. Further preprocessing of the time-frequency data like that could improve the SNR a great deal. The signal strength from the target can vary widely, especially as it moves closer or further away from the radar. The signatures intensity can vary quite a bit over time. In this thesis every time instant in the signature

is normalized to have almost the same maximum intensity. This method works quite well but can increase the noise dramatically if the target is lost momentarily for example if it is standing still and considered clutter. Instead of normalizing the signature itself the range-Doppler map could normalize its intensity based on the range. Each range bin would be multiplied by a different coefficient so that the varying intensity from the target will only be (in theory) from the radar cross section.

The gait-Doppler map is less effective when the average velocity of the target changes a lot and the target is spread in the Doppler spectrum. Estimating such a trend would give a good tool in estimating the targets average velocity, but could also be used to “normalize” the signature so that the fundamental gait-frequency can more easily be estimated. More features from the micro-Doppler signature should be investigated. For example the bandwidth of the signature.

## 4.2 Conclusion

The thesis has focused on and succeeded in developing algorithms and a system to extract micro-Doppler signatures from targets. Signatures from both humans and dogs has been produced and some simple features extracted from them. The major problem with the signatures created is that the radars pulse repetition frequency is a limiting factor and causes aliasing in the Doppler spectrum that corrupts the signatures. This has limited the study of targets to slow moving humans and dogs. Apart from the aliasing the signatures signal to noise ratio was good enough for tracking and the features investigated for both dog and human within the range of 4.4 meters. With the relatively slow targets being investigated it was found that the time windows used in the time-frequency analysis could be as long as 0.4 seconds although a shorter window is probably more useful. The experimental RELAX based micro-Doppler signature was developed and it has better time-frequency resolution but it is not clear that this would aid in any way with the classification problem. The features gathered from the STFT based signature seemed to perform just as well as the one from the RELAX based signature.

Three important features for classification was extracted from the micro-Doppler signature by calculating the gait-Doppler map. They are, i) the average Doppler frequency  $f_{av}$ (or average radial velocity  $v_{av}$ ), ii) fundamental gait frequency  $f_g$  and iii) the stride length  $L_s$  which is derived from the two former features. The result shows that it is possible to separate humans and dogs using these parameters see table 3.1. The reason is that since the dogs limbs are shorter than a human it also has shorter stride length at a specific speed. However, this is not enough features for an alarm system, since it can be easily fooled by a smart intruder that could for example take unnatural short steps and simulate a dogs combination of the aforementioned features. The way features are calculated is dependent on having 3 to 4 gait cycles available.

This is realistic, but to get a good estimate of the features it is a requirement that the average radial speed of the target does not change a lot during these cycles. This effect can probably be mitigated by preprocessing the signature before calculating the gait-Doppler map.

The Doppler frequency contains a lot of information about the target, and the micro-Doppler signatures attempts to brings forth all of the information contained in the Doppler shift. Signatures like the ones created in this thesis would be very useful in classifying different animals. Still, to create a truly robust classification system that can be used in a alarm and surveillance application, it may be easier to meet a specification by utilizing at least some of the range information and not only rely on the micro-Doppler signature.

# Bibliography

- [1] Terence W. Barret. “History of Ultra Wideband Communications and Radar: Part II, UWB Radars and Sensors”. In: *Microwave Journal* (Feb, 2001), pp. 22–46.
- [2] D. Chen and S. Qian. “Decomposition of the Wigner-Ville Distribution and Time-Frequency Distribution Series”. In: *IEEE Transactions On Signal Processing, Vol. SP-42* (Oct, 1994), pp. 2836–2842.
- [3] Victor Chen. *The micro-Doppler effect in radar*. Artech House, 2011.
- [4] Victor Chen. *Time-Frequency Transforms for Radar Imaging and Signal Analysis*. Artech House, 2002.
- [5] National Instruments. *STFT Spectrograms VI*. June 2008. URL: [http://zone.ni.com/reference/en-XX/help/371361E-01/1vanls/stft\\_spectrogram\\_core/#details](http://zone.ni.com/reference/en-XX/help/371361E-01/1vanls/stft_spectrogram_core/#details).
- [6] J.Li and P.Stoica. “Efficient mixed-spectrum estimation with applications to target feature extraction”. In: *IEEE Trans.Signal Process. vol. 44, no. 2* (Feb, 1996), pp. 281–295.
- [7] Changzhi Li et al. “Accurate Doppler Radar Noncontact Vital Sign Detection Using the RELAX Algorithm”. In: *IEEE TRANSACTIONS ON INSRTUMEN-TATION AND MEASUREMENT, VOL.59,NO.3* (March, 2010), pp. 687–695.
- [8] Jian Li and Zheng-she Liu. “Implementation of the RELAX Algorithm”. In: *IEEE Transactions On Aerospace And Electronic Systems Vol. 34, No. 2* (Apr, 1998), pp. 657–664.
- [9] Skolnik Merrill I. *Introduction to Radar Systems*. 3rd ed. McGraw-Hill, 2001.
- [10] Graeme Edward Smith. “Radar Target Micro-Doppler Signature Classification”. PhD thesis. University College London, 2008.

# Appendices

# Appendix **A**

## Selected Matlab code

Included here are some of the central Matlab code.

### A.1 The RELAX algorithm

```
function [eTheta, eAlpha] = RELAX(y, K, threshold, N_fft)
%Estimate the K dominating sinusoids in the signal y using
%threshold as threshold for convergence. N_fft is the length
%of the zero padded FFT signal

%Make sure y is in standard vector form
y_size = size(y);
if y_size(2)>y_size(1)
    y = y';
end
%Initialize
eAlpha = zeros(K,1);
eTheta = zeros(K,1);
N = length(y);
n = 0:N-1;
n = n';
f_step = 1/(N_fft-1);
f_limit = floor(N_fft/2);
for i=1:K
    count = 0;
    est_y_1 = zeros(N,1);
    for k = 1:(i-1)
        est_y_1 = est_y_1 + eAlpha(k)*exp(2j*pi*eTheta(k).*n);
    end
    y_diff = y-est_y_1;
    y_diff_fft = fft(y_diff,N_fft);
```

```
[~, theta_i] = max(abs(y_diff_fft));
%Correct Matlab indexes (it starts at 1) in the below if-else
if (theta_i) > f_limit
    eTheta(i) = f_step*(N_fft-(theta_i-1))*-1;
else
    eTheta(i) = (theta_i-1)*f_step;
end
%estimate alpha
eAlpha(i) = y_diff(theta_i)/N;
est_y_1 = est_y_1 + eAlpha(i)*exp(2j*pi*eTheta(i).*n);
cost1 = sum(abs(y-est_y_1));
convergence = false;
while ((convergence == false) || (count == 100))
    count = count+1;
    for k = 1:i
        est_y_2 = zeros(N,1);
        for p = [1:(k-1) (k+1):K]
            est_y_2 = est_y_2 + eAlpha(p)*exp(2j*pi*eTheta(p).*n);
        end
        y_diff = y-est_y_2;
        y_diff_fft = (fft(y_diff,N_fft));
        [~, theta_i] = max(abs(y_diff_fft));
        %Correct Matlab indexes (it starts at 1) in the below if-else
        if (theta_i) > f_limit
            eTheta(k) = f_step*(N_fft-(theta_i-1))*-1;
        else
            eTheta(k) = (theta_i-1)*f_step;
        end
        eAlpha(k) = y_diff(theta_i)/N;
    end
    %Calculate change in cost function
    est_y_2 = est_y_2 + eAlpha(i)*exp(2j*pi*eTheta(i).*n);
    cost2 = sum(abs(y-est_y_2));
    change = (cost1-cost2);
    if change < threshold
        convergence = true;
    else
        cost1 = cost2;
    end
end
end
end
```